Chapter 7
Analysis Techniques

7.1 Introduction

Nanomaterials, dispersed in the form of colloids in solutions, particles (dry powders) or thin films, are characterized by various techniques. Although the techniques to be used would depend upon the type of material and information one needs to know, usually one is interested in first knowing the size, crystalline type, composition, thermal, chemical state, and properties like optical or magnetic properties. A list of various commonly used techniques and their utility can be found in Box 7.1.

In this chapter, we shall briefly outline some of the techniques from those mentioned in Box 7.1.

7.2 Microscopes

Low dimensional materials such as quantum dots, quantum wires, quantum wells, self-assembled materials, interactions of small molecules with surfaces, multilayers etc. need special microscopes like Transmission Electron Microscope (TEM), Scanning Tunnelling Microscope (STM), Atomic Force Microscope (AFM) and Scanning Near-Field Optical Microscope. However, in many instances, one inspects the sample, specially thin films, with an optical microscope, to check the quality of samples like presence of cracks, agglomeration at large scale, etc. Therefore we shall begin with a simple optical microscope, define some common terminologies used in microscopy analysis work and then discuss other microscopes.

7.2.1 Optical Microscopes

Human eye perceives an object when visible light reflected from an object enters the eye. Size of an object observed by an eye depends upon the arc subtended by

S.K. Kulkarni, *Nanotechnology: Principles and Practices*,
DOI 10.1007/978-3-319-09171-6_7

the object at the lens and image on the retina of the eye. As illustrated in Fig. 7.1a, smaller the distance from the eye, bigger is the image of the object in the eye. There are, however, two limitations. An object kept at a distance smaller than ∼25 cm (this distance is known as the distance of distinct vision) from the eye cannot produce a sharp image of the object and other is that a human eye cannot detect an object smaller than ∼100 μm as a distinct object if placed close to another object. However, as shown in Fig. 7.1b, by placing a convex lens close to an eye, a magnified virtual image can be formed at a larger distance so as to form an image with larger angle θ′. Such a magnifying lens forms the simplest kind of microscope.

Box 7.1: Commonly Used Techniques in Materials Analysis

Microscopes

Optical microscope, Confocal microscope, Scanning Electron Microscope (SEM), Transmission Electron Microscope (TEM), Scanning Tunnelling Microscope (STM), Atomic Force Microscope (AFM), Scanning Near-Field Optical Microscope (SNOM).

Microscopes are useful to investigate morphology, size, structure and even composition of solids depending upon the type of microscope. Some of the powerful microscopes are able to resolve structures up to atomic resolution.

Diffraction Techniques

X-ray Diffraction (XRD), Electron Diffraction, Neutron Diffraction, Small Angle X-ray Scattering (SAXS), Small Angle Neutron Scattering (SANS) and Dynamic Light Scattering (DLS).

Scattering or diffraction techniques are often used in particle shape and average particle size analysis as well as structural determination.

Spectroscopies

UV-Vis-IR absorption (transmission and reflection modes), Fourier Transform Infra Red (FTIR), Atomic Absorption Spectroscopy (AAS), Electron Spin (or Paramagnetic) Resonance (ESR or EPR), Nuclear Magnetic Resonance (NMR), Raman Spectroscopy, various luminescence spectroscopies, Electron Spectroscopy for Chemical Analysis (ESCA) or X-ray Photoelectron Spectroscopy (XPS), Auger Electron Spectroscopy (AES).

Spectroscopies are useful for chemical state analysis (bonding or charge transfer amongst the atoms), electronic structure (energy gaps, impurity levels, band formation and transition probabilities) and other properties of materials.

Electric and Magnetic Measurements

Two or four probe measurements, Magnetoresistivity, Vibrating Sample Magnetometer (VSM), Superconducting Quantum Interference Device (SQUID), Magneto-Optical Measurements (Kerr and Faraday rotations).

(continued)

Box 7.1 (continued)

Measurement of resistivity is necessary for many applications. Magnetic and magneto-optical measurements throw light on the behaviour of the materials in presence of external magnetic fields.

Mechanical Measurements

Hardness, strength (Elastic moduli), Nanoindentation.

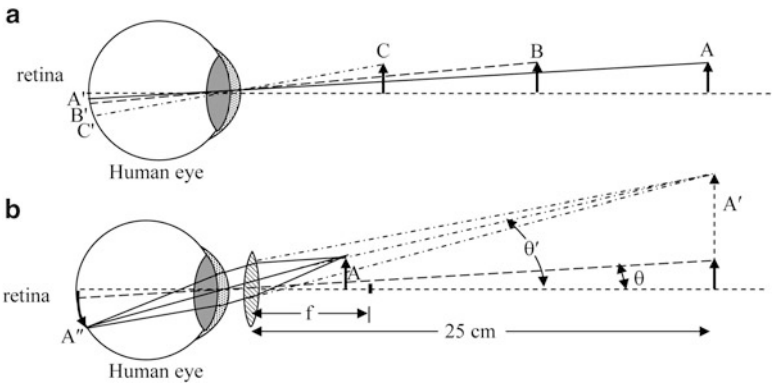

Fig. 7.1 (**a**) Size of the image depends on the distance from the eye. (**b**) By keeping a convex lens close to the eye, image of an object can be magnified

Magnification is defined as the ratio of angles subtended by the image (θ') to that (θ) by the object

$$M = \frac{\theta'}{\theta} \tag{7.1}$$

Magnification is approximately related to focal length f of the lens as

$$M \simeq \frac{25}{f} \tag{7.2}$$

where 25 in the numerator is the distance of distinct vision in cm and 'f' is the focal length of magnifying lens in cm.

An object would appear ten times larger with lens having $f = 2.5$ cm ($M = 25/2.5$) and is written as '10×'. When an image is 100 times bigger than the object, it is written as '100×' and so on.

With the magnifying ability of lenses in mind, Galileo invented in the year 1610 the simplest optical microscope. Currently used microscopes make use of at least two lenses viz. objective and eyepiece. Objective lens is the lens close to the object and eyepiece is close to the eye, as shown in Fig. 7.2.

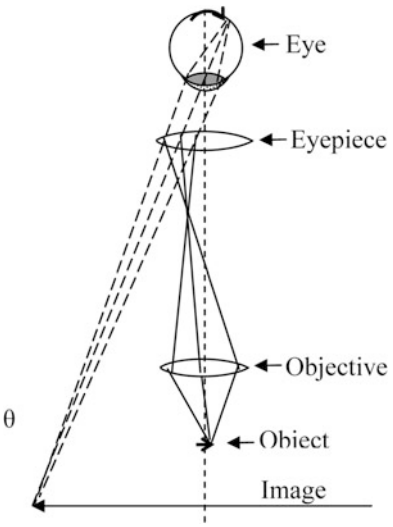

Fig. 7.2 Ray diagram of the simplest kind of an optical microscope using just two convex lenses

The objective lens (from a distance larger than its focal distance) forms the real image of an object, which in turn gets magnified as a virtual image due to eyepiece.

$$\text{Overall magnification } M = \frac{-x}{f_1}.\frac{25}{f_2} \tag{7.3}$$

where $-x/f_1$ is magnification due to objective lens and $\frac{25}{f_2}$ is the magnification due to eyepiece. Here 'x' is the distance of image from the focal point of the lens. Negative sign indicates that the image is inverted (Box 7.2).

Box 7.2: Resolution, Magnification and Depth of Focus of a Microscope
While using any microscope we should know its capabilities in terms of its resolution, magnification and depth of focus, which determine the extent to which we can get information about the samples under investigation. We shall discuss these below.

Resolution
It is the ability to produce two separate images of two closely spaced objects. The limit up to which the objects are resolved is determined by the diffraction of the waves. *Rayleigh criterion:* Maximum intensity of the peak due to one object should fall at the minimum intensity due to the other object.

(continued)

Box 7.2 (continued)
Magnification
It is the ratio of the size of the image to size of the object. Overall magnification is given by the product of magnification produced by various components of a microscope and camera factor.

$$M = M_o \times M_e \times M_c \times C$$

where M is overall magnification of the microscope, M_o – magnification due to objective lens, M_e – magnification due to the eyepiece, M_c is magnification due to change (if used) and C is camera factor.

Depth of Focus
It decreases with increased magnification. Sharpness of an image depends upon the numerical aperture '*NA*' and the refractive index n of the lens material.

It should be remembered that having large resolution is not sufficient. Magnification is also very important. A good microscope should have high resolution, sufficient magnification and adequate depth of focus.

In a commercial optical microscope more than two lenses, apertures, sample stage and light source are present in order to improve the quality of the observed image (lenses produce various defects in images like distortion, astigmatism etc. which can be partially corrected). Magnification of an optical microscope cannot be increased indefinitely as all the microscopes are limited by their ability to resolve the images to some limit. This is limited by the diffraction of the scattered light from an object. Two close-by areas on a sample can be considered as two apertures, the light passing through which can interfere to form a combined image. The closest distance between two points (or two areas), which can be seen as separate or resolved is given by

$$R = \frac{\lambda}{2n \sin \theta} \approx \frac{\lambda}{2NA}, \text{ for small values of } \theta \tag{7.4}$$

where λ is wavelength of light and θ is the semi cone angle of light entering the objective lens from the sample (or object) (see Fig. 7.2).

$NA = n \sin \theta$ is the numerical aperture of a lens with n as the refractive index of the lens. Approximating $NA = 1$, $R = \lambda/2$ which is often referred to as $\lambda/2$ limit or diffraction limited resolution. $\lambda/2$ limit is common to all microscopes based on the principle of scattering of waves, may be electromagnetic or those associated with particles.

Optical microscopes in general can resolve up to $\sim$0.2 μm as visible light ranges from 400 to 700 nm and the smallest wavelength, which can be used is 400 nm.

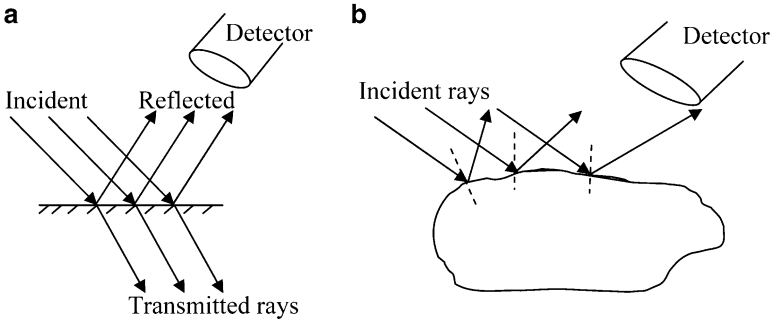

Fig. 7.3 (**a**) On a flat surface intense reflected beam will pass in the detector. (**b**) On a rough surface, due to scattering in different directions, the intensity of reflected beam passed in the detector would be less

In order to observe the images of objects, additionally, it is necessary to obtain sufficient contrast between the image of interest and its surrounding. This depends upon the method of illumination, absorption of light due to sample and some other factors like polarization of light etc.

When a beam of light is incident on a perfectly flat solid surface, it is known, following Snell's law, that it can get partly reflected and partly refracted (see Fig. 7.3a). However, if we consider a beam of light falling on a rough surface, as illustrated in Fig. 7.3b, then depending upon the surface roughness or morphology the intensity of the reflected beam can vary in different directions (Snell's law is obeyed but one needs to consider local normal to the surface) or the reflected beam would diverge.

This would mean that there would be an intensity variation from the sample surface. If the sample is having some grains or different optical properties (refractive index or reflecting power) for different parts of the sample surface, then intensity variations would occur and can be detected. The optical microscopes in the current use are equipped with a set of lenses to improve the sample illumination, sample movement stage, lenses with different magnification, camera with various apertures and other facilities to obtain high quality images as well as ease of operation.

7.2.2 Confocal Microscope

Resolution of an optical microscope can be improved by limiting the field of view. This is the principle used in a confocal microscope. A confocal microscope can be of transmission or reflection type. In Fig. 7.4, a ray diagram of a confocal microscope in transmission mode is illustrated. A point source of light and a small area detector are used in this microscope, which restrict the field of view. The light from the point source is focussed on the specimen to cover only a point (or very small area) on the sample. The objective lens in turn forms a small image of this illuminated portion on the point detector. It is possible to raster (move in x-y directions or in

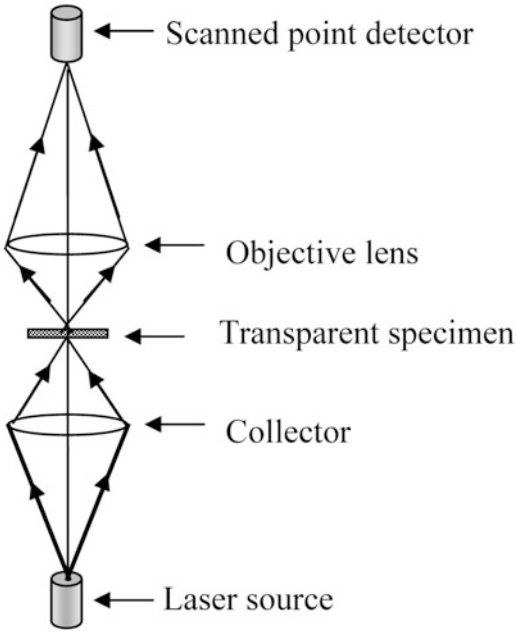

Fig. 7.4 Schematic diagram of a confocal microscope in transmission mode. Either specimen or beam falling on the specimen are synchronously rastered and image is reconstructed on the computer

a plane) the sample so that light falls on each part of the sample and the signal gathered by the detector is used to construct the image. Alternatively, the point source and detector are synchronously rastered to view the entire specimen and construct the corresponding image. Use of point source and detector improves the depth resolution of a confocal microscope. It is capable of optically sectioning a three dimensional thick object to a resolution determined by the detected sample volume. The detector uses an aperture which eliminates the light not coming from the focus on the sample and scans the sample in one plane point by point. Image of one plane is stored in a computer. By adjusting the focus of light in a different plane, point by point the entire plane is scanned and image of that plane is stored. Like this the sample is scanned to achieve high resolution 3-D image of the sample. Confocal microscope is therefore widely used in biology to study objects like cells.

7.3 Electron Microscopes

Electron microscopes bear similarity with optical microscopes. In optical microscopes, electromagnetic waves of appropriate wavelength scattered from the specimen are detected using a system of focussing lenses. In electron microscopes, electrons are used in place of electromagnetic radiation and electrostatic or magnetic lenses are used instead of glass lenses. According to wave-particle duality, electrons can sometimes behave as particles and sometimes as waves. Therefore, just like electromagnetic radiation, which can be used to image the objects, electron waves

Table 7.1 Wavelengths of electrons at some particular accelerating voltages

Applied voltage, kV	Wavelength in nm
20	0.0085
50	0.0053
80	0.0041
100	0.0037

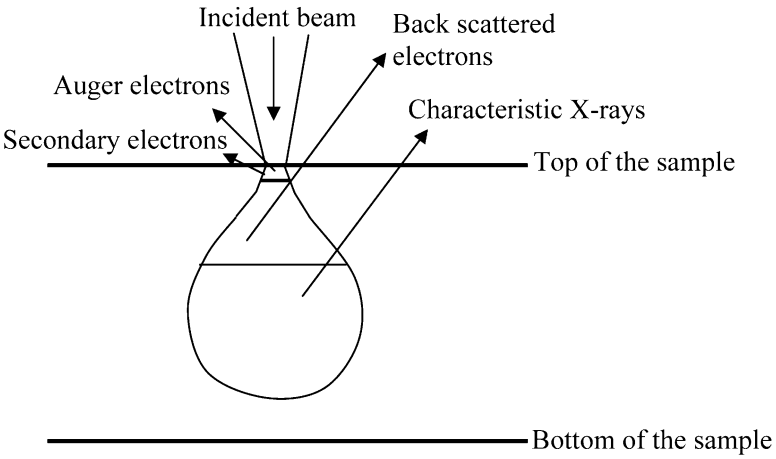

Fig. 7.5 Interaction of high energy electrons with solid

can be used to image the objects. Advantage of using electrons is that their wavelength can be tuned to a very small value, just by changing their energies so that the resolution can be increased. In Table 7.1 wavelengths of electrons at different energies are shown.

Wavelength can be simply calculated using de Broglie relation $\lambda = h/mv$ where h is Planck constant, m – mass of electron and v is the velocity of electrons. Velocity can be found out using $eV = ½\, mv^2$, where V is the applied voltage.

Although the wavelengths shown in Table 7.1 appear to be very small and one would have expected extremely high resolution, but in general the interactions between electrons and solid are quite complicated due to charge on incident electrons and subsequent interaction with electrons and ions in solids. As shown in Fig. 7.5, this interaction results into back scattering of electrons, production of Auger electrons, visible light, UV light and even X-rays depending upon the energy of the incident electrons, type of sample and thickness of sample. In any case, even a parallel beam of electrons after interaction with solid becomes defocussed as illustrated and in general, a focussed beam therefore forms a 'tear' shape volume of beam interaction zone.

There are two types of electron microscopes viz. *Scanning Electron Microscope (SEM)* and *Transmission Electron Microscope (TEM)*. Scanning electron microscope uses backscattered electrons from a sample for imaging and transmission electron microscope utilizes electrons transmitted through a sample. Obviously SEM can be used to image the surface of a thick sample but TEM needs to

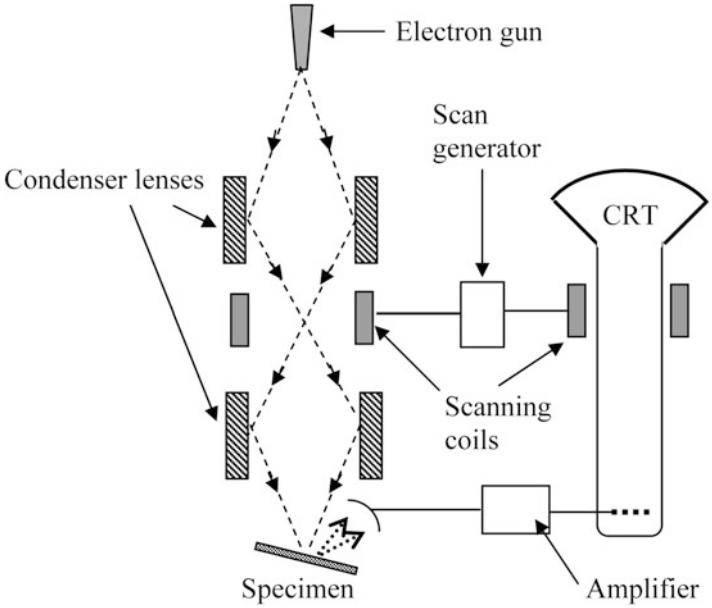

Fig. 7.6 A typical sketch of a scanning electron microscope. Electron gun, specimen and various electrodes etc. need to be mounted in a vacuum chamber

have a thin (maximum thickness ∼300 nm) sample so that high energy electrons can transmit through the sample. Both the microscopes use electrons which need to reach the sample without getting scattered by air. Therefore, the electron microscopes need vacuum for their operation.

In the following sections, we shall briefly study both SEM and TEM.

7.3.1 Scanning Electron Microscope

In Fig. 7.6, essential parts of a scanning electron microscope are shown. In an electron microscope, electrons emitted from a hot filament are usually used. However, sometimes cold cathode (a cathode that emits electrons without heating it) is also used. A cold cathode emits electrons under the application of a very high electric field. It is also known as a field emitter. Such SEMs are known as FE-SEM and are able to give better images than hot filament SEM. However, such FE-SEM is less common than hot cathode SEM.

In a scanning electron microscope, backscattered electrons or secondary electrons are detected (in some cases it is also possible to use sample current). Due to interaction of focussed beam with solid, the backscattered electrons are somewhat defocussed resulting into lowered resolution than one would expect.

In an electron microscope, the electron beam can be focussed to a very small spot size using electrostatic or magnetic lenses. Usually the electrostatic lenses are used

for a SEM. The fine beam is scanned or rastered on the sample surface using a scan generator and back scattered electrons are collected by an appropriate detector.

Signal from scan generator along with amplified signal from the electron collector generates the image of sample surface. In order to avoid the oxidation and contamination of filament as well as reduce the collisions between air molecules and electrons, filament and sample have to be housed in a vacuum chamber. Usually vacuum $\sim 10^{-2}$–10^{-3} Pa or better is necessary for a normal operation of scanning electron microscope. This makes electron microscopes rather inconvenient. However some manufacturers have been successful in marketing electron microscopes known as *environmental microscopes*, in which samples can be at rather high pressure of few hundreds of Pa (100–500 Pa). Sample preparation is therefore minimized and sample in biological conditions can be investigated. For this the electrons are accelerated as usual in a high vacuum system but they enter the sample chamber through a thin foil or aperture so that a large pressure difference can be maintained (Box 7.3).

Box 7.3: Ernst Ruska (1906–1988)

Ernst Ruska was born on 25th December 1906 in Heidelberg, Germany. He had his higher education at the Technical University of Munich. Around 1927 it was getting accepted that electrons have associated waves. Simple, back of the envelope calculation shows that high velocity electrons have waves having wavelengths which are four or five orders of magnitude smaller than that of the visible light. This led Ruska around this time to think that electrons can give much higher resolution than the usual optical microscopes. He therefore built electromagnetic lenses to focus electrons and used them to develop first electron microscope in 1933. In his microscope he used a thin specimen and electrons passed through towards a photographic plate producing a high resolution image.

(continued)

Box 7.3 (continued)
In 1937 Ruska joined Siemens-Reiniger-Werke AG and marketed in 1939 the first electron microscope. He remained with Siemens company until 1955 when he became the Director for Electron Microscopy Institute in Fritz Haber Institute of Max Planck Society in Berlin. He remained there as a Director until 1972. He shared with G. Binnig and H. Rohrer the Nobel Prize for Physics in 1986. E. Ruska died on 25th May 1988.

One disadvantage of electron microscopes is that insulating samples cannot be analyzed directly as they get charged due to incident electrons and images become blurred/faulty. Therefore insulating solids are coated with a very thin metal film like gold or platinum (<10 nm) making them conducting without altering any essential details of the sample. The metal film is usually sputter coated on the sample to be investigated prior to the introduction into the electron microscope. This enables even biological samples to be analyzed using an electron microscope. Additionally, some microscopes provide with a low energy electron flood gun to reduce the sample charging effect by providing more electrons to an insulating sample.

Electron microscopes can also be used to obtain the composition of sample using a technique known as Energy Dispersive Analysis of X-rays (EDAX). The high energy electrons striking the sample produce characteristic X-rays of atoms with which they interact. When analysis of the energies and intensities of such characteristic X-rays are compared one can obtain the composition analysis of the sample under investigation (Fig. 7.7).

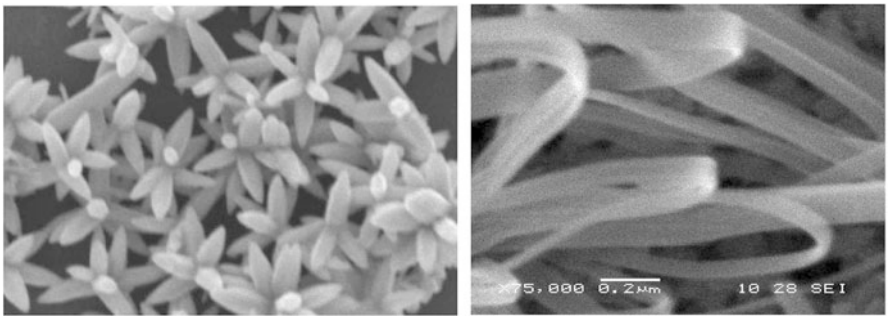

Fig. 7.7 Scanning electron microscopy images of ZnO with flower-like morphology and belt-like morphology. The chemical co-precipitation synthesis method has been used to obtain various morphologies by varying the synthesis parameters

7.3.2 *Transmission Electron Microscope (TEM)*

Transmission electron microscope is ideal for investigating the nanomaterials, as very high resolution is possible (better than ∼0.5 nm) using it. As the name suggests the electrons are transmitted through the specimen in this microscope. Electrons of very high energy (typically >50 keV) are used which pass through a series of magnetic lenses, as in an optical or SEM discussed earlier. Interaction of electrons with matter was also illustrated in Fig. 7.5. The basic components of TEM are electron source, condenser lens, specimen, objective lens, diffraction lens, intermediate lens, projector lens and a fluorescent screen in the given order. There may be some additional lenses in different microscopes in order to improve the image quality and resolution. The lenses are electromagnetic whose focal lengths are varied to obtain optimized images rather than moving the lenses themselves as is done in an optical microscope. Similar to SEM, the components (and specimen) of a TEM also have to be housed in a chamber having high vacuum $\sim 10^{-3}$–10^{-4} Pa for its proper functioning.

As illustrated in Fig. 7.8, TEM has the advantage that one can not only obtain the images of the specimen but also diffraction patterns, which enable to understand the detailed crystal structure analysis of the sample. Using diffraction analysis one can find out size dependent changes in the lattice parameters as well as defects in the sample. Figure 7.9 illustrates an example of SiO_2 nanoparticles and their corresponding diffraction pattern. Moreover it is also possible to analyze single

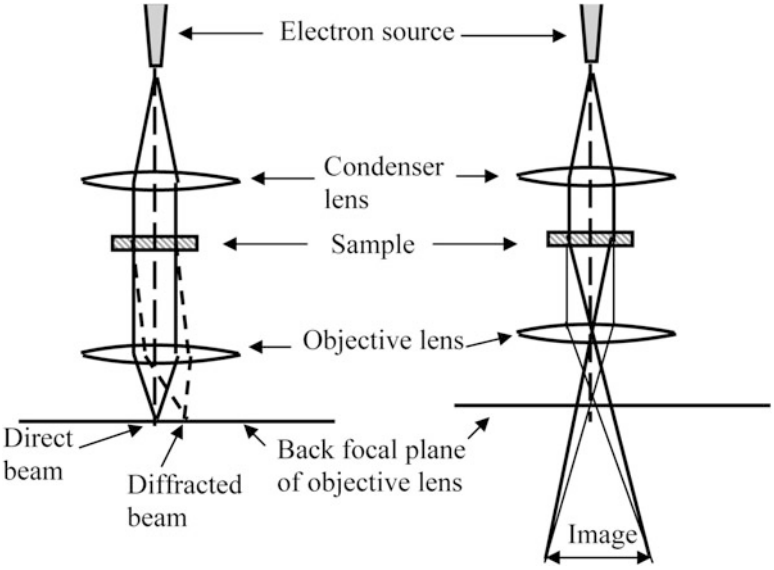

Fig. 7.8 Basic components of TEM

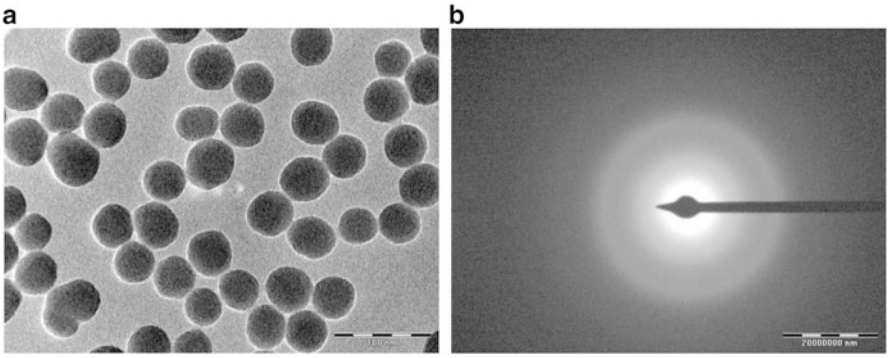

Fig. 7.9 SiO_2 nanoparticles image and diffraction pattern

particles of very small (nanometre) dimension. In some microscopes, it is possible to vary the sample temperature. This enables to investigate the problems such as size dependent melting point variation of nanoparticles (Box 7.4).

Box 7.4: Sample Preparation for Electron Microscopy

Sample preparation for electron microscopy can be quite a skillful and tedious job. For SEM, mostly sample thickness is not a problem as electrons are collected in the backscattering mode. In SEM, usually much lower electron energy is used as compared to that in TEM. Sample charging effect can be more severe in SEM and requires that insulating samples are coated with thin layer of some noble metal (Au or Pt, <10 nm) before the sample is introduced in the microscope chamber for analysis.

In case of TEM, as sufficient electrons need to be transmitted through the sample, thickness of the sample has a limitation. It becomes necessary to thin down the films (or multilayer samples) by proper grinding and/or ion etching as they might be deposited on some solid substrates. A technique like jet thinning is used for metallic samples and ion milling for non-conducting samples. Often the thin films are deposited on solid substrates. It becomes necessary to investigate then the cross sections. For biological samples a technique known as ultramicrotomy is used.

Powder samples (particle size <300 nm) can be held on some metal (usually copper) grid coated with a thin ($\sim$5 nm) carbon film or some polymer.

As both SEM and TEM require vacuum environment for their operation, sample degassing has to be avoided. Biological samples, therefore, have to be 'freeze dried' by some special process.

7.4 Scanning Probe Microscopes (SPM)

Scanning Probe Microscopes (SPM) is a generic name given to a family of microscopes in which a sharp tip of a metal is scanned across a sample surface in a raster mode to produce the images of samples even at subatomic resolution in some instances. The first SPM known as Scanning Tunnelling Microscope (STM) was developed around 1982 by G. Binnig and H. Rohrer for which they received Nobel Prize in 1986 along with Ernst Ruska. Subsequently many other SPMs like Atomic Force Microscope (AFM), Magnetic Force Microscope (MFM) and Scanning Near Field Microscope (SNOM) were developed to overcome some of the limitations as well as carry out 'spectromicroscopies' i.e. microscopy as well as spectroscopy combined in same instrument so that spectroscopy of same sample area is performed of which microscopy is performed. With spectromicroscopy, one is able to get not only the details of morphology and structure of a material but also know the chemical nature or electronic structure of the material and study mechanical, thermal, optical and magnetic properties too. Besides these benefits, great advantage is that unlike in electron microscopes, no special sample preparation is necessary nor vacuum is necessary unless one wants to carry out analysis of a clean surface. One can even use liquid environment for these microscopes. Thus it has been possible to investigate not only insulating but live or biological samples. Some of these microscopes and their modified versions can also be used for doing lithography and will be discussed in Chap. 9.

Here we shall discuss STM, AFM and SNOM, quite commonly used microscopes for nanotechnology work. In all these microscopes, scanning probe and raster principle are common. Probe is a fine metal tip of $\sim$10 nm diameter. Tip materials are Si, Pt-Ir or Pt-Rh. Even diamond film coated tips are used. Tips are obtained by etching a fine metal wire in some suitable chemicals or prepared lithographically. In case of microscopes like STM the tip is directly mounted on some specially designed piezo drive (or piezo tube). For AFM investigations, tip is mounted on a cantilever which is then mounted on a piezo drive. Function of a piezo drive is to scan the sample surface to be imaged. Materials like lead zirconium titanate (PZT) are known to be piezo crystals.

SPM scans are made over few nm to 100 μm in the horizontal plane (x-y) and about few nm to 10 μm in vertical plane (z). As shown in Fig. 7.10, starting at one point the scans are made by moving the tip on a line and then moving it to the next line. Digital images are collected at several points (pixels) like 64, 512 or 1,024 per line. Distance between two pixels determines the step size. Scanning is usually fast in one line going slowly to the other line. An image of the predetermined surface area is usually acquired in few minutes. Piezo drives along with the tip are very crucial in determining the resolution of the acquired images using SPM.

In order to achieve very high resolution like atomic level resolutions using SPM, it is essential that the microscopes be shielded from mechanical vibrations. As the

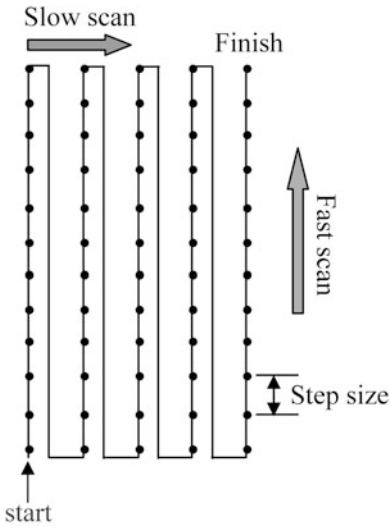

Fig. 7.10 Raster scan

currents (or forces) involved are very small, influence of external magnetic fields as well as electrical noise need to be avoided. Considerable efforts are usually made to avoid external disturbances by isolating the SPM using anti-vibration platform as well as using properly shielded electronics.

7.4.1 Scanning Tunnelling Microscope

As the name suggests, the scanning tunnelling microscope is based on the tunnelling principle (see Chap. 1). When two metals say M_1 and M_2 are brought at small distance (but larger than 10 nm) as depicted in Fig. 7.11a, even though their Fermi levels do not coincide, transfer of electrons from one metal to the other is not possible. To transfer electrons from one metal to the other, it is necessary for the electrons in the vicinity of the Fermi level to overcome the potential barrier known as the work function of the material. Typically, the work functions of metals are few electron volts (2–5 eV) and transfer of electrons at room temperature is forbidden. However, the metals brought in extremely close distance of the order of a few nanometres (usually less than 10 nm) behave differently. Electrons as shown in Fig. 7.11b can be transferred from one metal to the other to establish a common Fermi level without going over the potential barrier, set by the work function. At short distance of few nanometres, the wavefunctions of electrons from either side decay into the other metal. In other words, electrons can 'tunnel' from one metal to the other to occupy state of lower energy. This causes Fermi levels of the two metals to coincide with a small 'contact potential'. This reduces the barrier heights but changes are still small and barriers are sufficiently large for

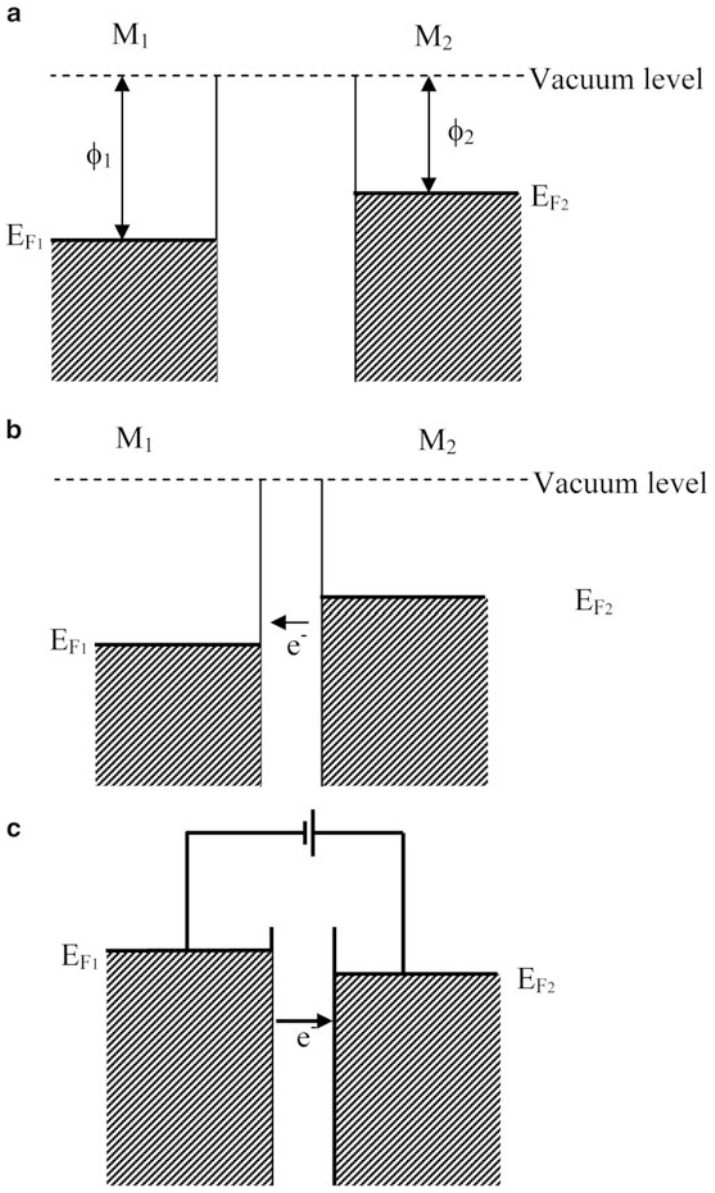

Fig. 7.11 Tunnelling of electrons from one metal to other. (**a**) Metals are at small distance, but not less than 10 nm. (**b**) Metals are in close contact with each other, at a distance less than 10 nm. (**c**) Potential is applied between two metals

electrons to overcome them. Once the Fermi levels coincide, the electrons cannot flow from one metal to the other. However, by raising the Fermi level of one metal with respect to the other, electrons can tunnel from one metal to the other, as shown in Fig. 7.11c.

The energy required by electrons to overcome the energy barrier is still very high and not obtained by applying the potential, but electrons can tunnel. The tunnelling probability or current depends upon the availability of the empty states in metal in which electrons flow (density of empty states) and distance between the two metals. Fermi level positions can be altered by applying a small voltage ($V < \varphi$) between the two metals. The metal (M_1) which is connected to the negative terminal of the power supply has raised Fermi level with respect to the other metal (M_2) whose Fermi level is lowered. This is made use of in an STM. As illustrated in Fig. 7.11c, the tip potential is made negative, therefore its Fermi level is raised and current flows from tip to the sample. Indeed it is possible to raise Fermi level of sample higher than the tip, so that electrons flow from sample to the tip. It is then quite obvious that by lowering the sample with respect to the tip and measuring the current flowing towards the sample, we are able to probe unoccupied states or empty energy levels of the sample. If the sample Fermi level is at higher level, electrons below Fermi level flow to the tip. Therefore, one can know about occupied states in the sample. Thus, STM is capable of performing even spectroscopy of occupied and unoccupied levels.

The tunnelling current is given as

$$I = C \exp(-kd) \tag{7.5}$$

where C is proportionality constant, d – the distance between two metals and k is known as decay constant. It is obtained as

$$k^2 = 8\pi^2 m \frac{(V_b - E)}{h} \tag{7.6}$$

where V_b is the difference between the Fermi level positions of the tip and the sample. E is the energy of the level to which electron tunnels.

Usually the distance between tip and the sample is between 0.5 nm to 1 nm and current of few picoamperes (pA) to nanoamperes (nA) is expected. It is quite clear from the Eq. (7.5) that current is very sensitive to the distance between tip and sample.

An STM can be operated in two different modes viz.

1. Constant current mode
2. Constant height mode

Constant current mode: Probe in the form of a sharp metal tip is moved slowly on the sample surface so that the current between the tip and the sample remains constant. In order to maintain the constant current between the tip and the sample, distance between the tip and the atomic corrugations also needs to be kept

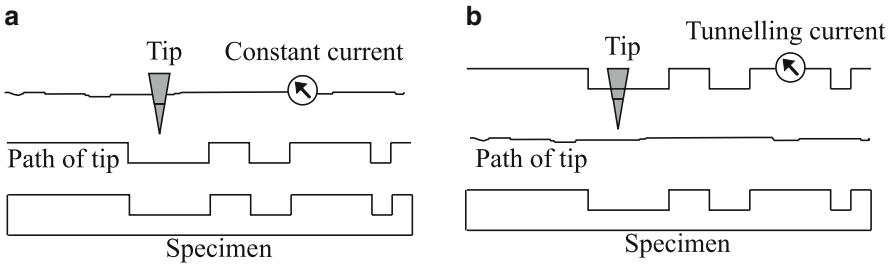

Fig. 7.12 (**a**) Constant current and (**b**) constant height modes

constant (see Fig. 7.12a). Thus the tip will have to follow the atom contours. By successively scanning the desired sample area in a raster mode, profile of surface atoms can be generated as an image, which is really the movement of the tip or the probe in an attempt to keep constant current between the sample and the tip, controlled by a proper feed-back loop. This is known as constant current mode.

Constant height mode: Alternatively, the tip can be moved on the sample surface at a constant height (typically >0.5 nm) as illustrated in Fig. 7.12b. As there is a relation given by Eq. (7.5), between current and the distance, a surface profile can be generated from the variations observed in the tunnel current. Thus the image is the replica of the variation of current as the tip scans the desired area of the sample surface. Advantage of the constant height mode as compared to the constant current mode is that the tip can be moved faster on the sample surface, as there is no necessity of the feed-back circuit. Besides it is dangerous to move the tip close to the sample in constant current mode, as that can occasionally hit some rough hillocks of the sample and get destroyed. This is avoided in the constant height mode and tip can be moved faster. However this would be at the cost of better sensitivity in the constant current mode.

Major limitation of STM is that the tunnelling current has to flow between the sample and the probe. Although the current is very small (of pico ampere order), it can be detected. However, in case of insulating samples, even this much current is not possible. Therefore, realizing this problem other scanning probe microscopes were developed (Fig. 7.13).

7.4.2 Atomic Force Microscope

Limitation of an STM is that it requires the sample to be a conductor or at least a semiconductor. This limitation was immediately realized and overcome by introducing Atomic Force Microscope (AFM) by G. Binnig and C. Gerber in 1985, quite immediately after the development of first STM. As discussed in Chap. 2, when two

Fig. 7.13 Photograph of a JSPM-5200 scanning probe microscope

atoms are close to each other, there are attractive and repulsive forces which depend upon the distance of their separation. Combined force is given by the equation

$$F = \frac{A}{R^{12}} - \frac{B}{R^6} \tag{7.7}$$

where F is resultant force between two atoms, A and B – constants and R is distance between two atoms.

The first term is the repulsive force and the second term is attractive force between two atoms. It can be seen that repulsive force is more effective at very short distance and changes rapidly with distance. This is due to repulsive interaction between the electron clouds at a short distance (Pauli exclusion principle).

AFM has a flexible cantilever ~100 μm long, 10 μm wide and 1 μm in height attached to a piezo drive. A tip is mounted on cantilever as shown in Fig. 7.14 which can be brought close to sample surface. For cantilever

$$F = K \cdot \delta z \tag{7.8}$$

where F is force experienced by the cantilever, K is related to the natural resonance frequency of the cantilever (spring constant) and δz is the displacement of the cantilever.

Resonant frequency of cantilever

$$(\omega_r) = \sqrt{\frac{K}{m}} \tag{7.9}$$

where ω_r is resonant frequency and m is mass of the cantilever.

If there is a gradient in force with distance,

$$F = F_0 + \left(\frac{\delta F}{\delta z}\right)\delta z \tag{7.10}$$

and

$$F_0 = \left(K - \frac{\delta F}{\delta z}\right)\delta z \tag{7.11}$$

Thus, the effective spring constant 'K' changes in the presence of gradient. Resonant frequency also correspondingly changes as

$$(\omega_r) = \sqrt{\frac{\left(K - \frac{\delta F}{\delta z}\right)}{m}} \tag{7.12}$$

The resonant frequency is used to control the tip-sample interaction.

AFM tip, in close vicinity of the sample surface, experiences a repulsive force which results into minute amount of bending of the cantilever. A laser beam is directed on back of the cantilever (see Fig. 7.14). Small deflections caused by the tip-sample interaction are recorded by a position sensitive photodiode. By rastering the probe on sample surface and measuring the cantilever deflections, surface image is obtained.

An AFM can be operated in three different modes viz. (1) Contact mode, (2) Non-contact mode and (3) Tapping mode.

Contact mode: In this case, the tip is in contact with the sample surface and is almost forced into it. However due to repulsive interaction between electron charge

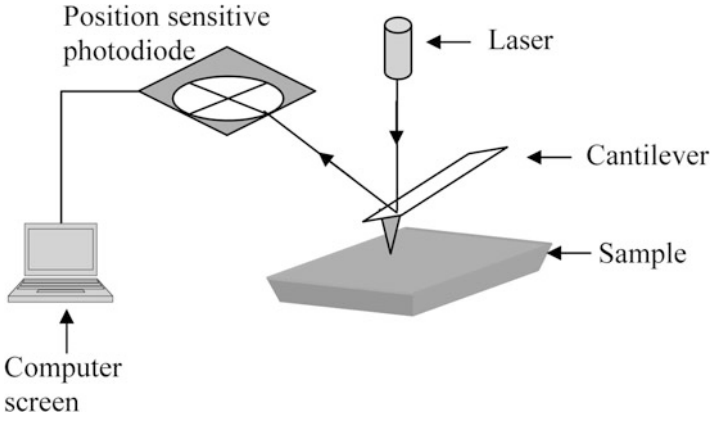

Fig. 7.14 Schematic of an Atomic Force Microscope

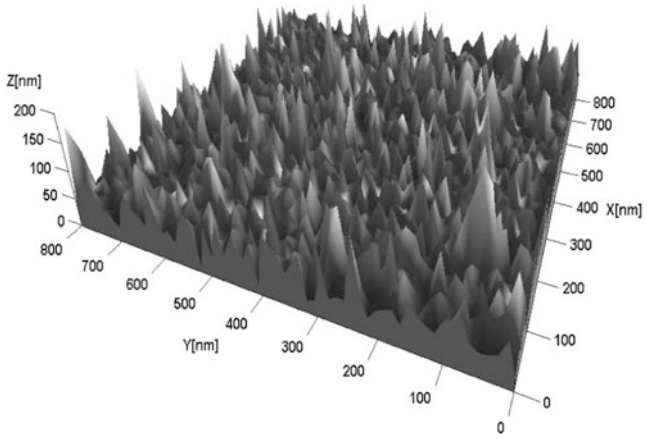

Fig. 7.15 An atomic force microscopy image of TiO_2 thin film deposited on silicon substrate

cloud of the tip atom and that of the surface atom, the tip is repelled back which bends the cantilever and deviates the direction of the laser beam. In this mode the interaction due to the first term on right hand side of Eq. (7.7) is dominant due to very small value of '*R*', the distance between two atoms. The main disadvantage of this mode is that the tip or sample can get damaged due to forcing of the tip into sample, especially, polymers or other organic materials like biological samples which can get damaged by this method.

Non-contact mode: In non-contact mode, the tip or the probe moves at some small distance away from the sample surface. Therefore, it cannot damage the sample. In this mode the second term on right hand side of the Eq. (7.7) is the dominant term. This term arises due to polarization of interacting atoms and is due to dipole-dipole interaction of two atoms (Fig. 7.15).

Tapping mode: Tapping mode is a combination of contact and non-contact modes. The resolution in contact mode is higher than that due to non-contact mode, because in contact mode the interaction between tip and surface atoms is much more sensitive to the distance as compared to that in non-contact mode. With tapping mode, high resolution advantage of contact mode and non-destructiveness of non-contact mode are achieved. The tip is oscillated in the vicinity of the surface at a distance of ∼50 nm in such a way that it nearly touches the sample during its cycle of oscillation. Tapping mode is simple and robust to use.

7.4.3 Scanning Near-Field Optical Microscope (SNOM)

The imaging in conventional optical microscope is based on the principle of interference of light waves. For this the object is first illuminated and then the scattered light by the object is collected so as to form the magnified image. The image of an object is reconstructed in the image plane.

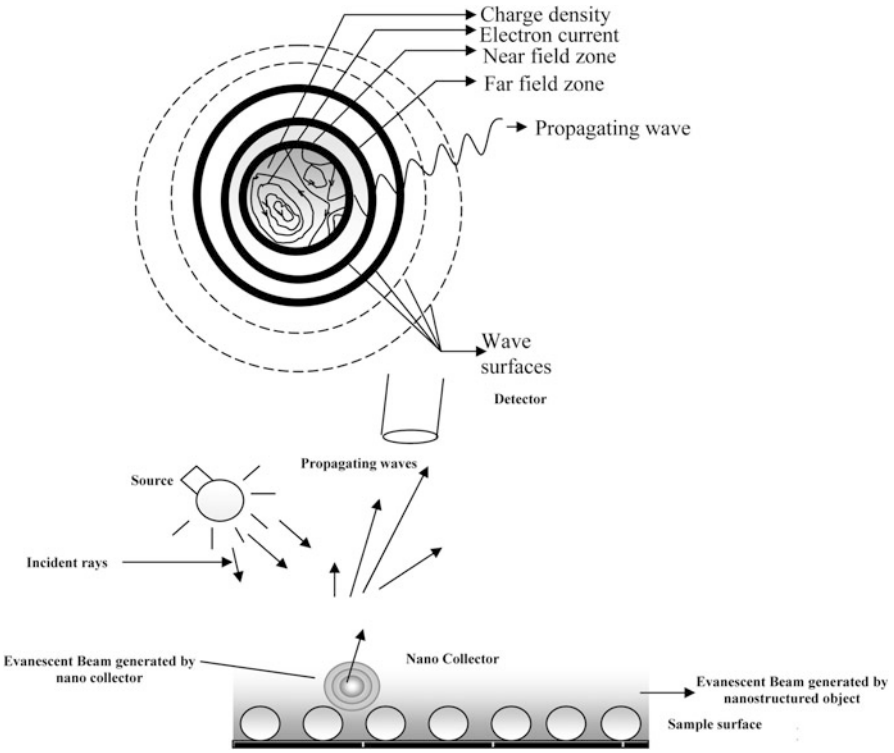

Fig. 7.16 Field of an object is shown. The electron currents and charge densities inside the object induce an electromagnetic field radiating from the surface. Far away from the surface, the field has the structure of propagating waves. Very close to the object, the field has a complex structure as it is composed of propagating and non – radiating components. Using a nanocollector i.e. an object like fibre with small diameter, changes in near field can be detected

In an optical microscope, the detector is kept at a very large distance of at least a few mm to cm from the sample. This is very large compared to wavelength of visible light normally used. For example if the wavelength of light used is ∼500 nm even the distance of 5 mm would be 10,000 times the wavelength of light.

It is known for a long time that the reflected light or the light leaving from a luminous object has two components viz. *evanescent* beam and *propagating* beam. This is shown schematically in Fig. 7.16. Evanescent beam is related to what is known as *near- field* and propagating beam is related to *far-field*. Near-field extends to very small distance and evanescent beam does not have a propagating wave nature. However photons cannot be trapped and must escape as propagating waves. This in fact is quite advantageous. If the near-field zone is disturbed, it also affects the far-field and propagating waves. This idea is used to overcome the diffraction limit and obtain a high resolution using scanning near-field optical microscope.

As shown in Fig. 7.17, a special probe with very small aperture of few nm diameter is brought very close to the sample surface.

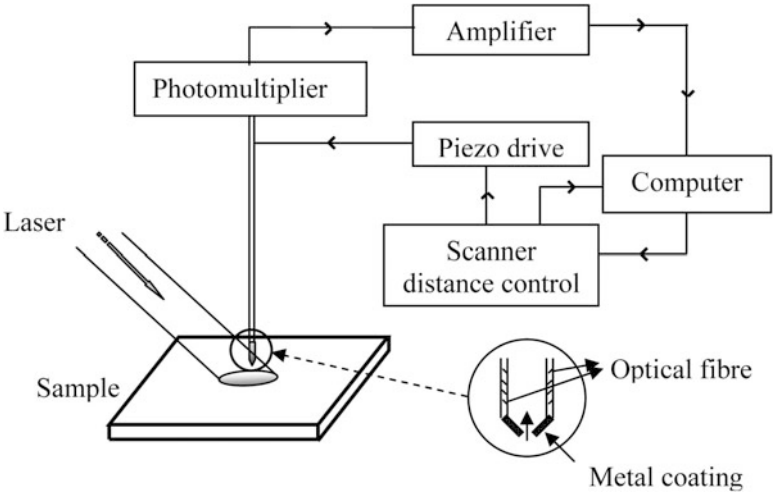

Fig. 7.17 SNOM probe and schematic of surface scan

The diameter of the aperture in the fibre as well as distance between the aperture and sample has to be smaller than the wavelength of light. Under such conditions, light leaves the sample before diffracting.

It can be readily appreciated now that the resolution obtained in a SNOM will depend upon the size of the aperture and the distance at which the probe can be placed. Thanks to the technological developments like availability of intense source like laser and fine movement of the probe using piezoelectric drive that high resolving power microscopy using SNOM is a reality. Very fine optical fibres are tapered to the diameter of less than 100 nm routinely and coated with some metal like aluminium. Metal coating of the fibre aperture is necessary because narrower is the aperture greater are the chances that the light can escape from the sides of the aperture wall. With current technology, apertures smaller than 100 nm can be routinely made out of glass fibre, achieving resolution even as good as ∼20–40 nm. In few cases resolution better than even 20 nm also has been achieved. Attempts are made to even overcome the limit due to aperture dimension. An Apertureless Near-Field Scanning Optical Microscope (ANSOM) has also been proposed. It is experimentally shown that ANSOM can resolve objects as small as 1 nm (Box 7.5).

Box 7.5: Photon Tunnelling

A scanning near-field optical microscope (SNOM) is sometimes also referred to as a photon tunnelling microscope. This idea is similar to that in STM. In an STM, electrons tunnel between tip and the sample under investigation. In order to observe the tunnelling current and use for imaging the distance

(continued)

Box 7.5 (continued)
between the probe and the sample has to be very small (<1–2 nm). By analogy, one can consider that if the distance between the sample and the probe is very small the photons tunnel. In an STM exponentially decaying electron tunnelling is sensed. In SNOM, photons leaving the exponentially decaying near-field are detected. Therefore, it is quite reasonable to think of SNOM as 'Photon Scanning Tunnelling Microscope (PSTM)'.

In Table 7.2, a comparison is made of various microscopes described in this section. Magnification and resolution numbers are given to indicate typical expected values and can vary from model to model (Boxes 7.6 and 7.7).

Table 7.2 Comparison of various microscopes

Microscope (radiation/interaction used)	Magnification	Resolution
Human eye (visible light)	–	100 μm
Optical microscope (UV-Vis-IR)	10^3	0.1 μm
Scanning electron microscope (electrons)	10^5–10^6	3 nm
Transmission electron microscope (electrons)	$>10^6$	0.1 nm
Scanning tunnelling microscope (electron current)	$>10^6$	0.1 nm
Atomic force microscope (e-e repulsion)	$>10^6$	0.1 nm
Scanning near-field optical microscope (vis light)	10^5	20–50 nm

Box 7.6: History of SNOM
As early as in 1928, E.H. Synge wrote a short note to the *Philosophical Magazine* (Volume 6, Dec 1928, p. 356) suggesting a method for extending the resolution of an optical microscope to about 0.005–0.004 μm. He mentioned that the method was suggested to him by a distinguished physicist (without mentioning the name). He, however, wrote about the difficulties in having intense source of light, adjusting distance between the sample and the source close to $\sim 10^{-6}$ cm and creating the aperture for light source as small as $\sim 10^{-6}$ cm diameter. It can be appreciated that in the absence of lasers and piezoelectric devices at that time, the practical realization of SNOM was not possible.

Ash and Nicholls (*Nature* 237 (1972), 510) demonstrated the resolution which was not limited by incident wavelength. However, they used microwaves to demonstrate the principle of near-field microscopy.

(continued)

Box 7.6 (continued)

Success of the near-field concept in microwave region led Pohl and others (*Appl. Phys. Lett.* 44 (1984), 651) to demonstrate SNOM in the visible light range. They could produce the resolution as high as 25 nm with a wavelength of 488 nm.

Box 7.7: Optical Stethoscope

Pohl et al. (*Appl. Phys. Lett.* 44 (1984), 651) have compared the SNOM with the doctor's stethoscope. A doctor can locate the position of the heart to within less than 10 cm by moving the stethoscope over the patient's heart and listening to the sound of heart beat. If the frequency of heart beating can be considered to be in the range of 30–100 Hz, its wavelength would be in the range of almost 100 m. Thus the stethoscope provides a resolving power of $\sim \lambda/1000$. Such a high resolution has become possible because of the smallness of the probe (the end of stethoscope) as well as its placement at a distance much smaller than the wavelength (100 m) from the object (heart) to be examined.

The concept of stethoscope can be applied for other wavelengths and other types of waves. An optical stethoscope which allows image recording with sub wavelength resolution was further demonstrated by Pohl et al. in their paper.

7.5 Diffraction Techniques

We discussed in the previous section some microscopy techniques. These techniques are useful to understand the surface morphology of the samples under investigation. In cases where atomic resolution is achieved one can know about surface structures too. However, knowledge of bulk structure is normally not possible using these techniques. Diffraction techniques using electrons, X-rays or neutrons produce information about crystal structure, and are used to understand structure (Bravais lattice) of bulk materials and can be extended to investigate nanomaterials. However the usual diffraction analysis relies on the long range periodic arrangement of atoms/molecules. For larger nanoparticles (>20 nm or so, sufficient long range order is established). While investigating very small particles (<20 nm) special precautions need to be taken as will be discussed from time to time. We shall discuss here only the X-ray diffraction technique as electron or neutron diffraction are similar to some extent and can be very well understood once X-ray diffraction is studied.

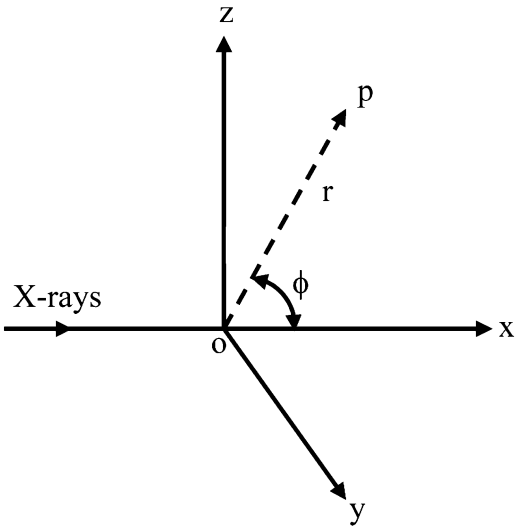

Fig. 7.18 Thomson's explanation of scattering of X-rays by electrons located at origin. Intensity is measured at point P

7.5.1 X-Ray Diffraction (XRD)

We are able to see objects around us as light is scattered by the objects and enters our eyes. Similarly, X-rays scattered by atoms enable us to understand about arrangement of atoms in solids. As early as in 1912 von Laue postulated that if X-rays are waves and distances between atoms in solids are comparable to wavelength of X-ray, then they should be diffracted by atoms in solid.

When we say that X-rays are scattered by atoms we really mean that they are scattered by electrons of atoms. It was shown by J.J. Thomson that if unpolarized X-rays are incident on free electrons, located at the origin O (see Fig. 7.18), the scattered intensity at point P is given as

$$I_e = \frac{nIe^4}{2r^2m^2c^4}\left(1 + \cos^2\phi\right) \tag{7.13}$$

where I_e is intensity of X-rays at point P, e – charge of an electron, I – intensity of the X-ray beam falling on a free electron at the origin, r – distance of point P from the origin, n – number of electrons, m – mass of an electron, ϕ – angle between incident beam and scattered beam and c is the velocity of light.

Above equation indicates that I_e is proportional to $1/m^2$. It is easy to convince therefore that nucleus, which is much heavier than an electron will not be able to scatter X-rays. It is also clear that most of the beam will be scattered in the forward direction and the intensity in other directions would be very small. Intensity also reduces drastically away from the scattering electrons as $1/r^2$.

7.5.2 Atomic Scattering Factor

It is also evident from Eq. (7.13) that more is the number of electrons (n), more would be the scattered X-ray intensity. An atom with atomic number Z has Z electrons in it. However in atoms we do not have the situation assumed by Thomson viz. free electrons. The scattered intensity, however, is proportional to Z, X-ray wavelength and angle of scattering. This is known as atomic scattering power.

Scattering power of an atom is referred to as atomic scattering factor f and is defined as

$$f = \frac{\text{Amplitutde of wave scattered by an atom}}{\text{Amplitutde of wave scattered by a single electron}} \tag{7.14}$$

It can be shown that

$$f = \frac{z \sin \theta}{\lambda} \tag{7.15}$$

where Z is atomic number, θ – half the angle between incident beam and scattered beam direction and λ is wavelength of X-rays.

Further, it is the interference of scattered rays that is important. If the scattered rays are either in or out of phase, their amplitudes will either add or cancel each other. If, however, there is no phase relation between the atoms then intensities would simply add. Consider, for example, an ensemble of N atoms of a gas in a closed vessel. As the atoms of a gas are in continuous motion, without any regular arrangement of atoms, each atom scatters X-rays but there is no definite phase relation amongst them. Scattered intensity from an atom is proportional to square of amplitude of the rays. If A is the amplitude of the incident rays, intensity scattered by each ray would be A^2. As there are N atoms, total intensity scattered by gaseous atoms would be NA^2. On the other hand if there is a correlation between the phases of N atoms each scattering wave of amplitude A, then amplitudes would add up to give a total amplitude of value NA. The intensity would be given by $(NA)^2$. Thus the intensity would be N times larger than that from uncorrelated atoms (Box 7.8).

Box 7.8: Laue Pattern

Laue with his collaborators placed in front of a single crystal of $CuSO_4$ a photographic plate and allowed a narrow beam of X-rays to pass through the crystals as illustrated in Fig. 7.19. He observed well defined diffraction spots on the photographic plate. Today this kind of arrangement is still used, replacing the photographic plate with X-ray detector, to study the crystals and is known as 'Laue Method'.

(continued)

Box 7.8 (continued)

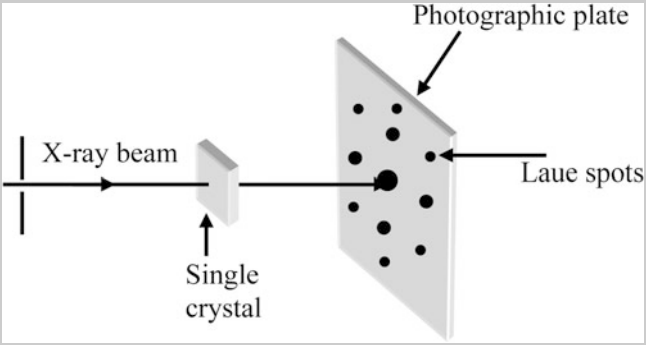

Fig. 7.19 Arrangement to obtain Laue photograph

In the same year (1912), as Laue performed diffraction experiments, W.H. Bragg and his son W.L. Bragg studied structures of a number of crystals like NaCl, KCl, KBr etc. to verify the Laue method.

W.L. Bragg also offered a simple geometrical explanation of observed diffraction pattern. This is now known as 'Bragg condition' or 'Bragg Law' and is discussed here.

7.5.3 Bragg's Law of Diffraction

Bragg considered that a beam of X-rays falls on crystal planes at some grazing incidence, θ, as shown in Fig. 7.20.

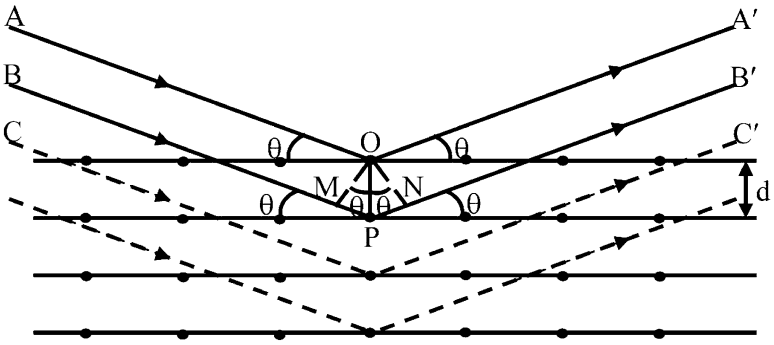

Fig. 7.20 Geometrical explanation of X-ray diffraction

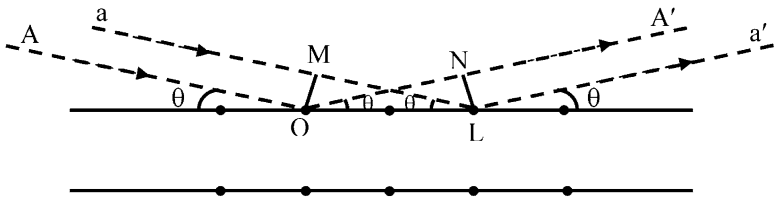

Fig. 7.21 Diffraction from the surface atoms

Beam of parallel rays is assumed. Consider that parallel rays AO and BP are incident on atoms at O and P respectively making an angle θ. Rays are scattered as OA′ and PB′. Distance between O and P is '*d*' (distance between the consecutive planes).

The path difference between AOA′ and BPB′ is

$$\text{Path difference} = \text{MP} + \text{PN} = 2\ \text{OP}\ \ \sin\theta = 2\,d\ \ \sin\ \theta \tag{7.16}$$

If λ or multiple of λ is the path difference between ray AOA′ and BPB′, they will reinforce or interface constructively.

$$\text{Therefore, } n\lambda = 2d\ \ \sin\ \theta, \text{ where } n = 1, 2, 3 \ldots \tag{7.17}$$

n is known as order of diffraction. Equation (7.17) is Bragg diffraction condition. In most of the cases only $n = 1$ is considered.

Consider now, parallel rays AO and aL falling on the first row of atoms at a grazing angle θ and scattered rays OA′ and La′ as shown in Fig. 7.21. The rays OA′ and La′ are also parallel to each other and make grazing angle with the surface. OM and LN are perpendiculars on aL and OA′ respectively.

$$\text{Path difference} = \text{ML} - \text{ON} = \text{OL}\cos\theta - \text{OL}\cos\theta = 0 \tag{7.18}$$

Thus OA′ and La′ scattered from the first plane are able to interfere constructively as they are in phase. Thus all atoms at the surface receiving radiation at angle θ will interfere constructively.

Consider now the rays AOA′ and CQC′ diffracted from 1st and 3rd planes respectively as in Fig. 7.22. Between AOA′ and CQC′

$$\text{Path difference} = \text{M}'\text{Q} + \text{QN}' = 2d\ \ \sin\ \theta + 2d\ \ \sin\ \theta = 4d\ \ \sin\ \theta$$

In order that rays reinforce constructively, they should be multiples of wavelength. If path difference is 2λ,

$$2\lambda = 4d\ \ \sin\ \theta \Rightarrow \lambda = 2d\ \ \sin\ \theta$$

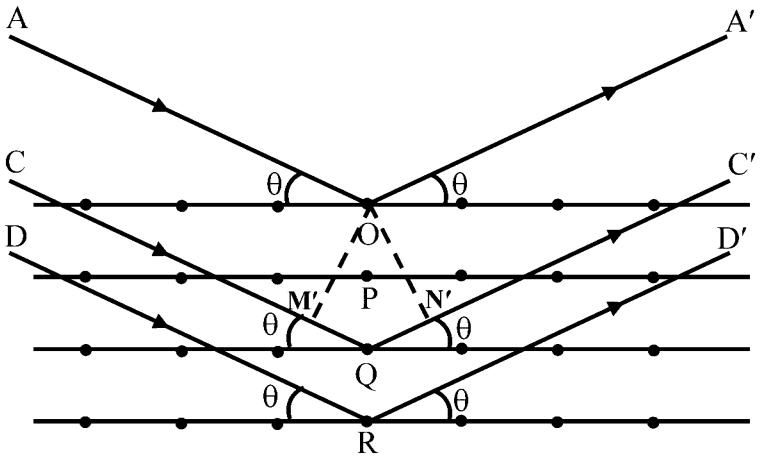

Fig. 7.22 Rays scattered from different planes, in same direction make constructive interference

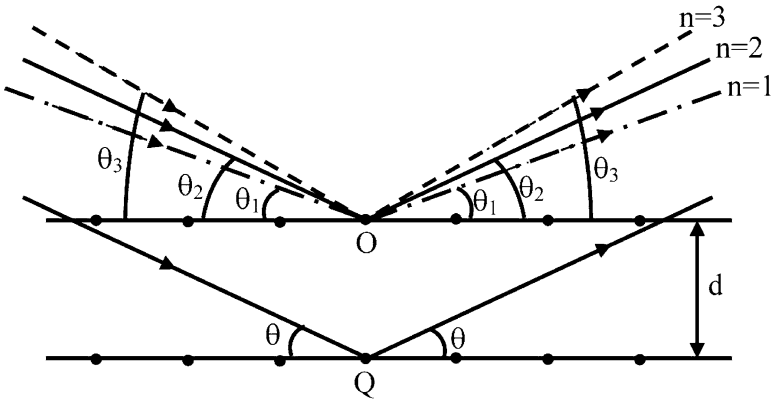

Fig. 7.23 Given set of planes can diffract for same wavelength of X-rays in different directions to satisfy Bragg law

For rays AOA′ and DRD′ have to interfere in same direction, path difference has to be 3λ.

i.e. $3\lambda = 6d \sin\theta \Rightarrow \lambda = 2d \sin\theta$ and so on.

Thus rays scattered by those in different planes in same direction will all reinforce to give constructive interference.

Consider now a situation as in Fig. 7.23, if λ and d are fixed, for angle θ_1, $\lambda = 2d \sin\theta_1$, will be satisfied for $n = 1$ i.e. path difference is just λ.

But for another angle θ_2, path difference can be 2λ. Still constructive interference can take place but in another direction. Thus

$$2\lambda = 2d \ \sin\ \theta_2 \ (n = 2) \tag{7.19}$$

For yet another angle θ_3 the condition

$$3\lambda = 2d \sin\theta_3$$

must be satisfied.

Consider following numerical example

Let $\lambda = 1.5$ Å and $d = 3$ Å .

For $n = 1$ and angle θ_1, using Bragg's law, we get, $\theta_1 = 14.50°$.

$$\text{For } n = 2, \theta_2 = 30°$$

Thus keeping λ and d constant we can get diffraction in different orders (n) from a set of planes at angles θ_1, θ_2, θ_3 .... Only condition will be $\theta < 90°$.

7.5.4 Diffraction from Different Types of Samples

So far we considered the diffraction from a set of planes, assuming them to be infinite in number. We may have samples which are single crystalline, polycrystalline solids, liquids or even gases. Amorphous solids, liquids, gases and nanocrystalline materials do not have infinite ordered arrangement of atoms but have few atoms and few planes (small single crystals or crystalline nanomaterials). Nanoparticles with disordered structure can be treated like amorphous bulk solids. In Fig. 7.24 the differences in scattering of X-rays by different materials are shown.

It can be seen from Fig. 7.24 that in case of a monoatomic gas (like He, Ar, Kr etc.) forward scattering occurs without any diffraction peaks in any other direction. In case of liquids or amorphous solids one or two peaks at angles other than the angle of incidence appear due to short range order in these materials. For single crystals, diffraction peaks appear at various angles. Intensities of peaks depend upon atomic scattering factor as well as crystal structure (or form) factor which we shall consider in the following section. The diffraction peaks from ideal single crystals are sharp, and broadened to certain extent only by instrumentation factor. However in case of polycrystalline sample the peaks are broadened due to the size of the grains. All the grains in crystal may not be of the same size. Therefore the width of the diffraction peaks can be considered as the effect of convolution of different peaks giving the average grain size. The diffraction peaks are broadened in case of nanoparticles also due to small number of atoms and planes present in them. We shall discuss this in a following section and show how one can determine the average particle size using the widths of diffraction peaks.

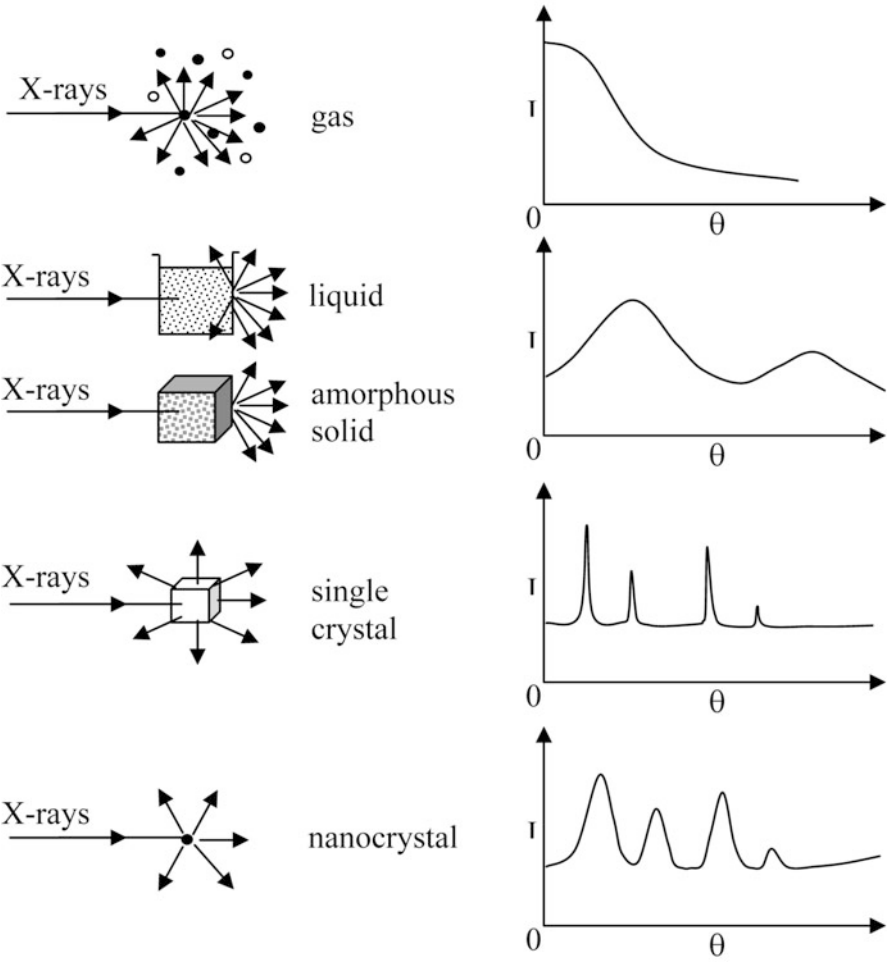

Fig. 7.24 Diffraction from gases, liquids, solids and nanocrystals

7.5.5 Crystal Structure Factor

The intensity of diffracted X-rays from different planes even from a perfect single crystal cannot be same. Different planes in unit cell of a crystal have different number of atoms. Due to specific arrangement of atoms in crystals (characteristic of material), it so happens that the X-rays scattered from different atoms may not be in phase. Therefore intensities of X-rays from different planes can be shown to be given by what is known as crystal structure or crystal form factor *F*. Crystal structure factor is also related to atomic scattering factor *f*. Crystal structure factor is defined as follows.

$$|F| = \frac{\text{Amplitude of waves scattered from all atoms in a unit cell}}{\text{Amplitude of waves scattered by an electron}} \tag{7.20}$$

$$= \sum_{P}^{N} f_p e^{2\pi i(hu+kv+lw)} \tag{7.21}$$

where sum is over all atoms, P to N, u, v and w denote the coordinates of atoms in unit cell and h, k and l are Miller indices.

Intensity of a diffraction peak is $|F|^2$.

It can be easily verified that in some unit cells systematic absence or enhancement of diffraction intensities from different planes can occur due to crystal structure factor.

7.5.6 Diffraction from Nanoparticles

We know that in a nanoparticle number of atoms is very small. Nanoparticles cannot be considered as an infinite arrangement of atoms as is usually assumed in Solid State Physics, in order to determine various properties of solids. In case of amorphous nanoparticles, similar to an amorphous bulk solid material, broad diffraction peaks are expected to occur. However in case of nanoparticles in which atoms do have ordered lattices some changes in diffraction are to be expected as compared to single crystal or polycrystalline bulk solid diffraction (often the nanoparticles are similar to single crystals and do not have grain boundaries). It has been found that the diffraction peaks in nanocrystalline particles are broadened compared to single or polycrystalline solid of the same material. This effect can be understood as follows.

Consider a limited number of planes say 0, 1, ... m or total $m+1$ planes in a set. Note that here first plane is numbered as 0. Let d_{hkl} be the interplaner distance. If the thickness of the crystal is say t then $t = m\ d_{\text{hkl}}$. Let the X-rays of a single wavelength λ fall on the set of planes d_{hkl}. All the rays in a beam may not be exactly parallel to each other. As shown in Fig. 7.25, rays AO, BP, ..., LS only are parallel and make angle θ_B with parallel planes (hkl). Let these rays scatter coherently and interfere constructively to satisfy Bragg's diffraction condition. This should produce an extremely sharp peak widened only due to instrument limitation. However ray like CO is at slightly larger angle than θ_B and so is the ray MS striking the mth plane. Both CO and MS are parallel to each other. It can be understood that the ray like CO cannot interfere constructively with rays parallel to it just in 1st, 2nd etc. planes. But there would be a plane say m at which it interferes constructively (corresponding to thickness of crystal). Therefore

$$(m+1)\,\lambda = 2T\ \sin\ \theta_1 \tag{7.22}$$

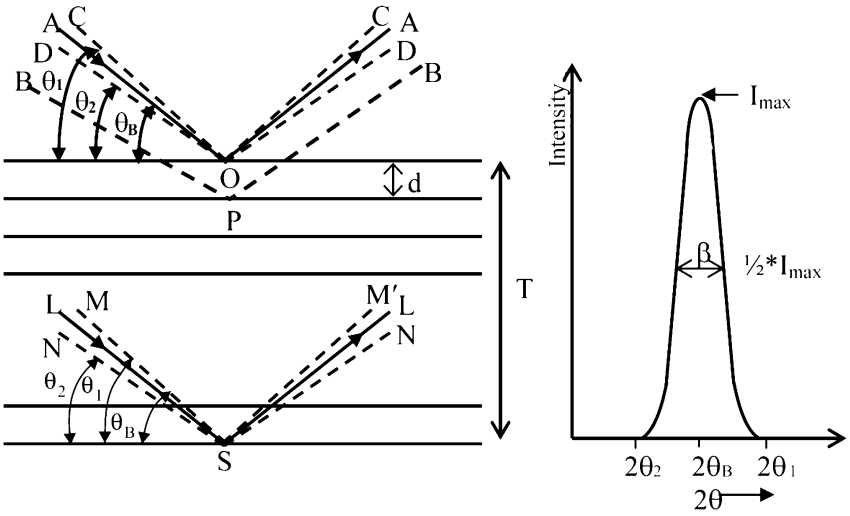

Fig. 7.25 Effect of crystal size on the diffraction

and for ray such as DO let the constructive interference occur just one plane before the *m*th plane. Therefore

$$(m-1)\,\lambda = 2T \sin\ \theta_2 \tag{7.23}$$

Subtracting (7.23) from (7.22), we get

$$\lambda = T\,(\sin\theta_1 - \sin\ \theta_2) \tag{7.24}$$

Therefore

$$\lambda = 2T\ \cos\left(\frac{\theta_1+\theta_2}{2}\right)\sin\left(\frac{\theta_1-\theta_2}{2}\right) \tag{7.25}$$

$$\text{as}\left(\frac{\theta_1+\theta_2}{2}\right) = \theta_B \text{ and } \sin\left(\frac{\theta_1-\theta_2}{2}\right) = \frac{\theta_1-\theta_2}{2} = \frac{\beta}{2} \tag{7.26}$$

Thus we get

$$\lambda = 2.T.\frac{\beta}{2}.\ \cos\theta_B \tag{7.27}$$

Therefore,

$$T = \frac{\lambda}{\beta\ \cos\theta_B} \tag{7.28}$$

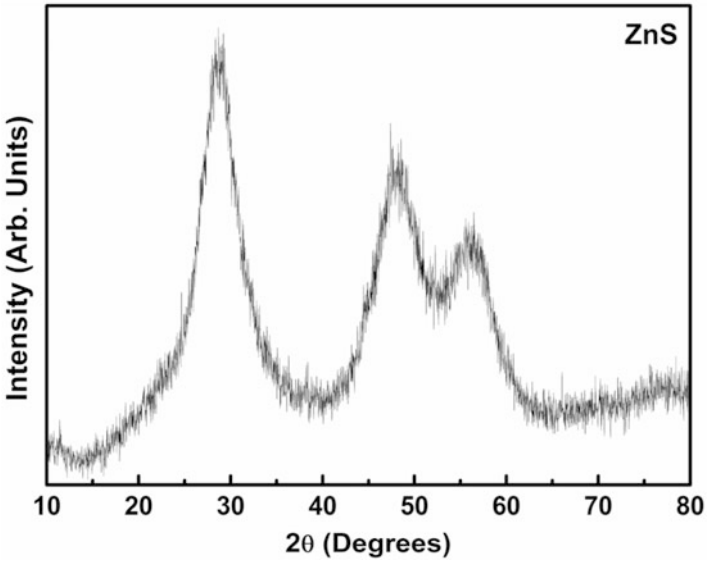

Fig. 7.26 X-ray diffraction pattern of ZnS nanoparticles

More accurate form of the equation for spherical nanoparticles is

$$T = \frac{0.9\,\lambda}{\beta\ \cos\theta_B} \tag{7.29}$$

This is known as Scherrer equation. The width β is the broadening caused by nanoparticle size. Scherrer formula can be used to evaluate the average particle size smaller than $\sim$100 nm which is just what is needed in nanoscience. However for extremely small particles ($<$2 nm), the broadening of diffraction peaks may become very large so that they resemble the peaks in an amorphous solid. Under such conditions, the peaks may result from convolution of peaks due to different planes also and unambiguous size determination is prohibited. For example, consider Fig. 7.26 in which the diffraction peak at 30° due to ZnS nanoparticles is so much broadened that it is not possible to decide whether it is the convolution of three planes viz. of a hexagonal lattice structure or it is a size broadened peak of a zinc blende structure. In such situations, another method known as Debye Function Analysis is adopted. In order to determine the shapes of nanoparticles, study of self-assembly in particles, multilayers etc. additional techniques like Small Angle X-ray or Neutron Diffraction (SAXS or SANS), X-ray Reflectivity or Neutron Reflectivity are available. Such techniques require intense X-ray sources such as rotating anode or synchrotron radiation and will not be discussed here. For neutron scattering, neutrons available from a nuclear reactor or special spallation sources are used.

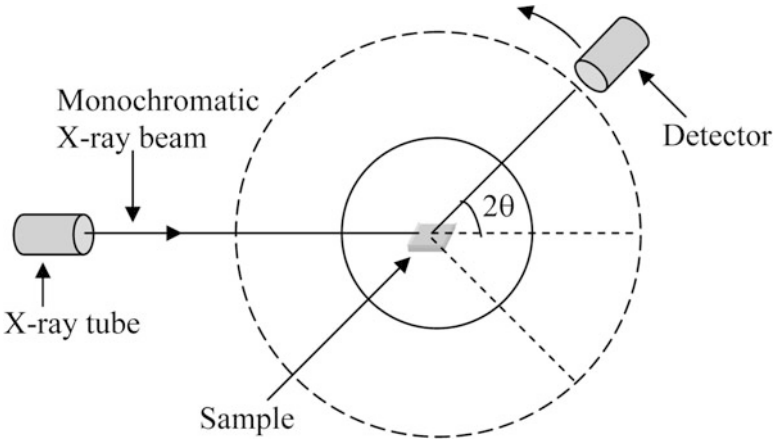

Fig. 7.27 Schematic of X-ray diffractometer

7.5.7 X-ray Diffractometer

There are different types of X-ray diffractometers available for crystal structure analysis. Same can be used for nanomaterials analysis. The most commonly used diffractometer is known as Powder Diffractometer or Debye-Scherrer Diffractometer after its inventors. This diffractometer is conceptually simple and allows quite an accurate determination of crystal structure of polycrystalline samples, thin films and nanoparticles.

As illustrated in Fig. 7.27 it consists of a monochromatic source of X-rays, usually from a copper target or anode giving CuK_{α} ($\lambda = 0.154$ nm after passing through nickel filter), sample holder and an X-ray detector. Both sample and the detector move around an axis passing through sample centre and normal plane of the paper.

Some times sample heating/cooling facilities are provided.

The diffracted rays make an angle 2θ at the detector with respect to incident beam direction. A plot of intensity (counts) as a function of angle 2θ (usually 20°–160°) is a diffraction pattern ready for analysis. For most of the routine work, this is quite sufficient. Detector is a suitable photon counter like Geiger Muller tube, proportional counter, scintillation counter or solid state detector. Usually, due to finite size of X-ray beam ~1–2 mm^2, smaller angles (<20°) are not accessible using these diffractometers. However for some detailed analysis of thin films or nanoparticles where additional information can be obtained at as small as θ ~0.1°–0.2°, modifications of Debye Scherrer Diffractometer or another diffractometer is needed.

7.5.8 *Dynamic Light Scattering*

It is a technique capable of determining the 'hydrodynamic' size of the particles. Hydrodynamic size can be defined for a particle of irregular shape as the effective size of a particle when it is dispersed in a liquid. For spherical particles, the hydrodynamic size is same as the actual particle size with radius say R.

Dynamic Light Scattering (DLS) technique is also known by various names like Photon Correlation Spectroscopy (PCS), Quasi Elastic Scattering, Diffusive Light Scattering, 3-D Dynamic Light Scattering, Beating Spectroscopy, Homodyne Spectroscopy and Intensity Fluctuation Spectroscopy. However, DLS and PCS are the names which are more common in use.

The DLS technique, unlike microscopy techniques like SEM, TEM, STM and AFM as discussed previously in this chapter, is capable of determining the particle size or size distribution only when the particles are dispersed in some liquid. The technique depends on the intensity fluctuations of visible light scattered from the particles while they make random Brownian motion in the liquid. It is basically Rayleigh scattering and size of the particles has to be much smaller than the wavelength of light used as a source.

When a beam of intense and monochromatic coherent beam like laser light falls on a small volume of liquid, the scattered light intensity measured by a detector at certain angle θ with respect to the direction of the incident beam depends on the angle θ, wavelength of light λ and refractive index n of the medium. The scattering vector value is given as

$$q = \frac{4\pi n}{\lambda} \sin\left(\frac{\theta}{2}\right) \tag{7.30}$$

The scattering geometry is depicted in Fig. 7.28. If the scattering from each particle occurs only once, the analysis becomes straightforward. Therefore multiple scattering events are avoided using dilute samples or small concentration of particles

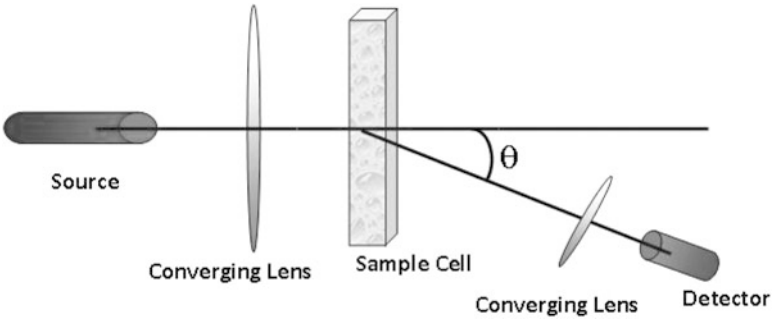

Fig. 7.28 Light scattering geometry

in the liquid. It is known from the Stokes-Einstein relation that the diffusion coefficient of particles with radius R is given by

$$D = \frac{kT}{6\pi\eta R} \tag{7.31}$$

where k is Boltzmann constant, T – temperature of the liquid and η is viscosity of the liquid.

As the particles move randomly in the liquid, their scattered intensities at the detector also change randomly or fluctuate. This is because the observed intensity of light from a given volume of liquid depends upon the interference of light being scattered from randomly distributed particle of the irradiated volume. The intensity at any instance, therefore, depends upon the relative positions of the particles or phase differences. If the intensity fluctuations due to random motion of particles are analyzed on a time scale smaller than the time taken by the particles to move the distance of the incident wavelength λ, then one can find that movements of the particles are still correlated. Obviously if the intensities are measured after a very long time the positions would not be correlated. When the measurements are made on a very short time scale, the particle position would not change drastically. As more and more time elapses the correlation would become less and less. Correlation decays exponentially. The exponential decay is related to the diffusion of particles and through Eq. (7.31) to the particle size. If the particles are monodispersed, a single exponential function is expected. Statistical analysis of the intensity fluctuation can be made using the following equation.

$$g^1(t) = \exp\left(-q^2 D_t\right) \tag{7.32}$$

where $g^1(t)$ is the first order normalized autocorrelation function, q is the scattering vector length defined by Eq. (7.30) and D is the diffusion coefficient in the equation. By measuring $g^1(t)$ at one scattering angle, diffusion coefficient (hence particle radius R) of particles can be obtained. If the measurements can be done over a range of scattering angles, plot of corresponding $g^1(t)$ against q^2 gives a straight line, slope of which yields D, the diffusion coefficient.

If the particles are not monodispersed, the first order correlation function $g^1(t)$ would depend upon more than one diffusion coefficients. If D_i is the diffusion coefficient of the ith particle, $g^1(t)$ can be written as

$$g^1(t) = \sum_{i=1}^{n} \exp\left(-q^2 D_i\right) A_i \tag{7.33}$$

where A_i denotes the weight or amount of each component. A common method used to analyze the polydispersed particles is 'cumulants method'. Here $g^1(t)$ is expanded and written as

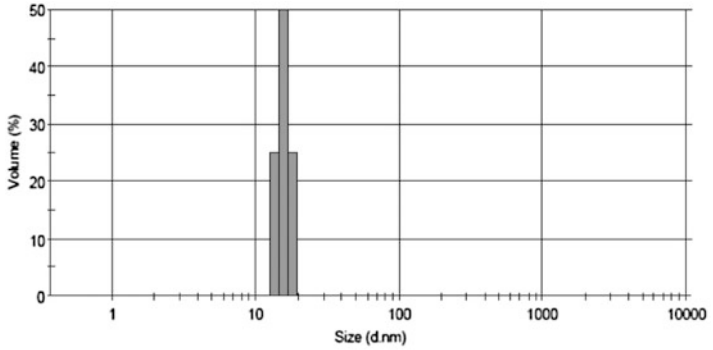

Fig. 7.29 Size determination of PbS nanoparticles using a Dynamic Light Scattering equipment

$$g^1(t) = \exp\left(-q^2 D_t\right)(1 + K_1 + K_2 + \ldots) \tag{7.34}$$

$K_1, K_2 \ldots$ are the first, second etc. cumulants.

The experimental set up is very simple as schematically shown in Fig. 7.28 and the commercial instruments are equipped with determining the autocorrelation function including cumulant method. They are able to give information of diffusion coefficients as well as particle size distribution over a wide range of ~1 nm to 10 μm size. Usually a beam of laser light is necessary, as concentration of particles in the solution has to be kept low in order to avoid the multiple scattering effects. One also tries to use efficient detectors like avalanche photodiode so that good signal is obtained. Figure 7.29 depicts a typical size distribution obtained for PbS nanoparticles obtained from such a DLS set up.

7.6 Spectroscopies

7.6.1 Optical (Ultraviolet-Visible-Near Infra Red) Absorption Spectrometer

Optical absorption spectroscopy is a very useful technique to study metals, semiconductors and insulators in bulk, colloidal, thin film and nanostructure forms. Semiconducting as well as some insulating materials have an optical energy gap. When the energy of photons is insufficient to excite electrons (see Fig. 7.30) from valence band to conduction band, no absorption takes place. At some critical photon energy, a sudden rise in absorption occurs as energy of photons is just sufficient to excite the electron to conduction band minimum. At still shorter wavelengths or higher energy photons continue to get absorbed. The absorbed (or reflected) intensity as a function of wavelength from ultraviolet (~200 nm) to near infra red (~3,000 nm or many a times only up to 1,000 nm) is useful to understand electronic structure and transitions between valence and conduction band of materials.

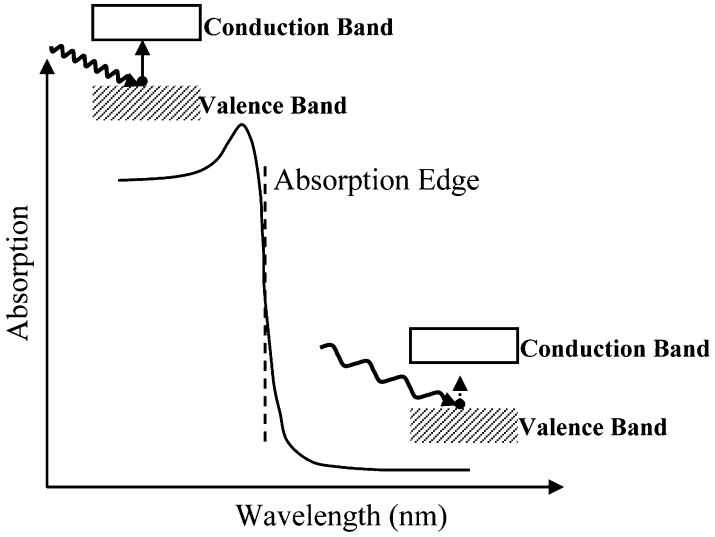

Fig. 7.30 Schematic optical absorption spectrum (semiconductor)

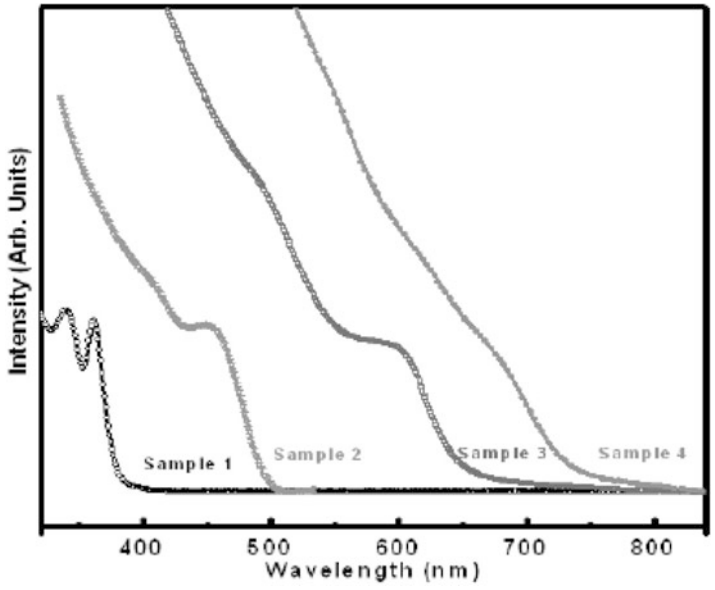

Fig. 7.31 Absorption spectra of CdSe nanoparticles

For nanomaterials with reduction in the particle size characteristic of materials a shift in the absorption edge can occur. The shift is usually to shorter wavelength and therefore known as *blue shift*. The theory of size dependent energy gap changes is discussed in Chap. 8. Figure 7.31 shows size dependence of absorption spectra

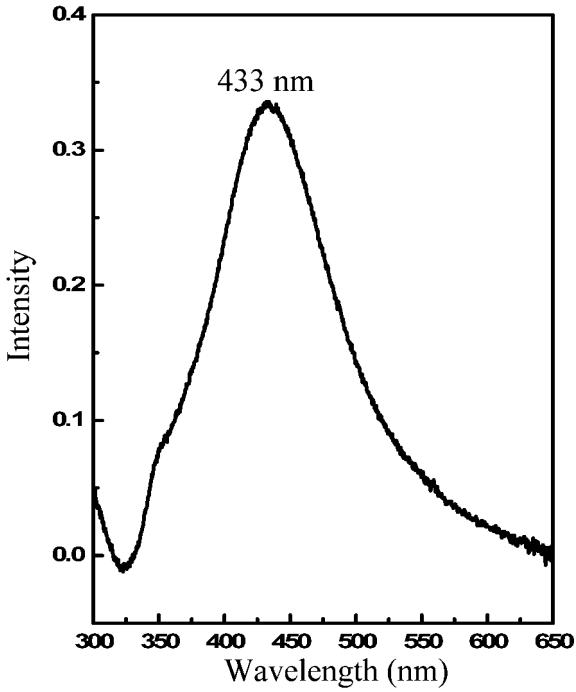

Fig. 7.32 Optical absorption due to silver nanoparticles

for CdSe nanoparticles. Note that absorption of bulk CdSe should have started at ∼730 nm as bulk CdSe has an energy gap of 1.7 eV at room temperature.

In case of metal thin films or particles like gold or silver, one may have strong surface plasmon resonance (more details in Chap. 8) due to resonant absorption of photons. Peaks are also expected in the range of UV-Vis-NIR range. The peaks are broad and their positions are size dependent. They too show blue shift with reduction in the particle size. Peak widths for both metal or semiconductor nanoparticles depend upon the size as well as size distribution of particles. See Fig. 7.32 for silver nanoparticles.

UV-Vis-NIR absorption spectroscopy is, therefore, a useful technique to analyze nanomaterials. Here we shall briefly discuss the essential parts of an experimental set of a UV-Vis-NIR spectrometer.

7.6.2 UV-Vis-NIR Spectrometer

The experimental set up in principle is very simple. A high intensity lamp (or change of lamps in different spectral regions) giving radiation from UV to NIR region is required. A monochromator selects different wavelengths, which fall on the sample. Depending upon its properties, the sample reflects or absorbs certain wavelengths and transmits the rest. The transmitted (or reflected) intensity at different

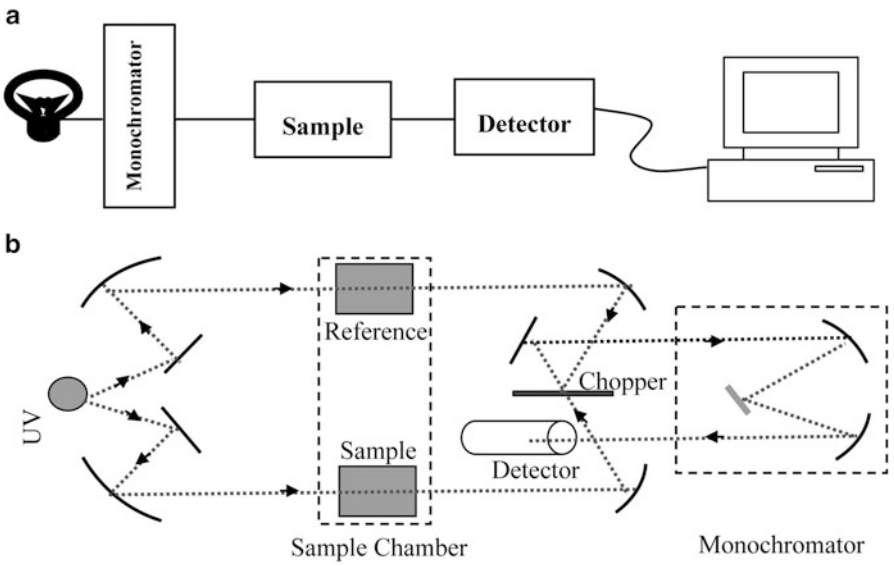

Fig. 7.33 (**a**) Schematic of UV-Vis spectrometer. (**b**) Schematic of dispersive spectrometer

wavelengths are detected by a photodetector and given as an input to a recorder or computer. When the monochromator signals corresponding to selected wavelengths falling on the samples are the signals for X-axis and photodetector signal for Y-axis, absorption plots as shown earlier in Figs. 7.31 and 7.32 are obtained. Figure 7.33a illustrates the schematic of the spectrometer. In practice it is advisable to use a reference, so as to eliminate the effect of path traversed by photons in sample holder, solutions in which colloids are suspended etc. Therefore beam from the radiation source is split into two parts. One part traverses through the reference compartment (cuvett) and through the nanoparticles dispersed in a liquid forming the sample under analysis. The reference is a liquid which is used to disperse the nanoparticles, without actually having nanoparticles. The intensities of light from reference and sample are finally compared to give the signal only due to the sample. A schematic of a typical double beam spectrometer is given in Fig. 7.33b.

Usually H_2 discharge lamp, deuterium lamp or tungsten lamp are used. Common monochromators are gratings or prisms. Photon detectors that are normally used are photomultiplier tube or photodiode. Liquid sample holders are usually made up of quartz glass.

7.6.3 Infra Red Spectrometers

We have seen earlier that inorganic nanomaterials are often surface passivated with organic molecules or sometimes they form composites with organic materials.

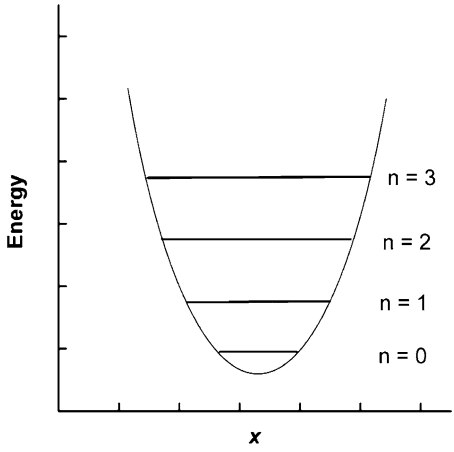

Fig. 7.34 Vibration levels in a molecule

Identification of such molecules often throws light on the processes occurring at the surface of nanomaterials. Many functional groups like –OH, –SH, =C =O, $–CH_2$, $–NH_2$ etc. have some characteristic absorption bands in the Infra Red regions.

Molecules have characteristic vibration energy levels as schematically shown in Fig. 7.34. Characteristic absorption bands for the molecules occur as molecules undergo transitions from their one characteristic energy level to another.

The allowed energies of vibration levels are given as

$$E_n = (n + 1/2)\, h\upsilon_o \tag{7.35}$$

where n are the quantum numbers for vibrations and take the values 0, 1, 2, 3 . . . and υ_o is the frequency of oscillator. The transition occurs by absorption of photon following the selection rule $\Delta n = 0$. For the infra-red absorption to take place, the molecules have to have a dipole moment. The molecules are then said to be IR active. Thus an H_2O molecule is IR active and would show characteristic absorption band. However symmetric CO_2 molecule does not have any permanent dipole on it. Hence CO_2 is not IR active.

It is useful to perform infra red spectroscopy of nanomaterials to find out if there are any active molecules present. Infra Red band is roughly divided into three regions viz. Near Infra Red (912,500 cm^{-1} to 4,000 cm^{-1}), Infra Red (4,000 cm^{-1} to 400 cm^{-1}) and Far Infra Red (400 cm^{-1} to 10 cm^{-1}).

There are two types of infrared spectrometers in common use. One is simple dispersive spectrometer and is often just referred to as IR spectrometer and the other is Fourier Transform Infra Red Spectrometer or FTIR spectrometer. FTIR spectrometer is mainly used to simultaneously record the entire wavelength range thus reducing data acquisition time as well as improving the signal to noise ratio. FTIR does not have any monochromator to select wavelengths. The dispersive IR

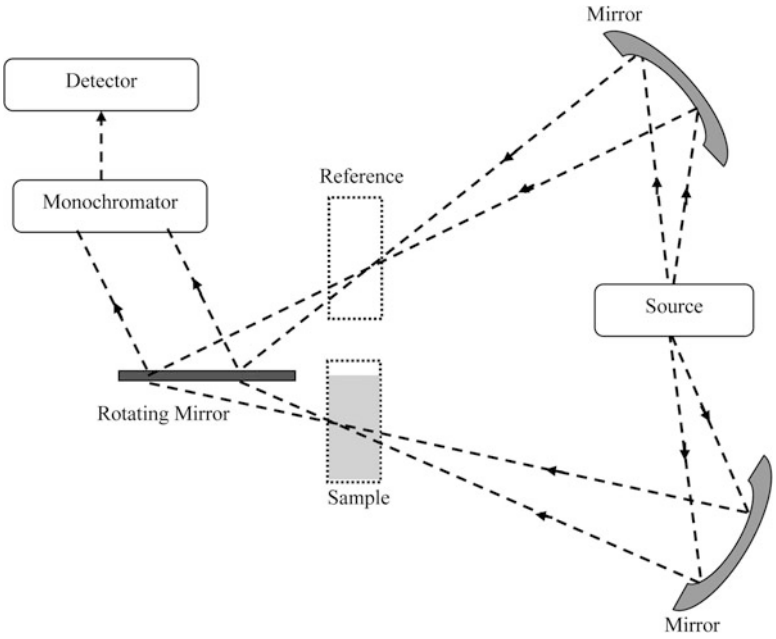

Fig. 7.35 Schematic of Dispersive IR Spectrometer

spectrometer uses either grating or prism as a monochromator to select the wavelength and sequentially scan the spectrum. We shall discuss both the spectrometers in the following sections.

7.6.4 Dispersive Infra Red Spectrometer

Figure 7.35 illustrates schematically a dispersive type IR spectrometer. It consists of an IR source, sample compartment, chopper, monochromator, focusing and collimating mirror and an IR detector. There are slits located at various points in the path of the beams so as to control the size of the beam.

An IR source is a tungsten lamp, Nernst glower or nichrome coil and high pressure mercury arc lamp depending upon whether NIR, Mid IR or Far IR region is to be investigated. Spectrometers are usually able to switch between different lamps.

IR detectors may be photoconductive cells, thermopiles, thermistors, Golay or pyroelectric, depending upon the range of wavelengths to be detected. The beam of IR from a single source is usually spilt into two and allowed to pass through the slits, then on reference sample and the actual sample. Reference sample signal can be subtracted from sample spectrum signal so as to eliminate effects due to sample

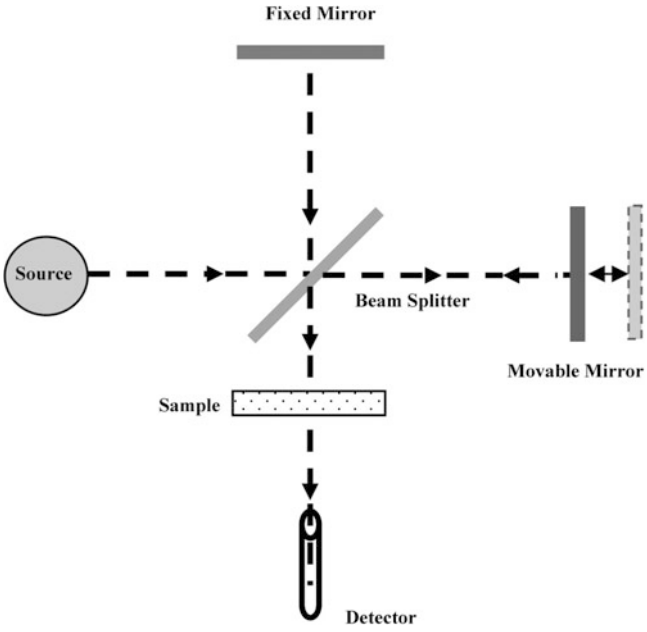

Fig. 7.36 Schematic of Michelson interferometer

preparation. Chopper cuts beam either from sample or from reference alternately so that each beam falls on gating (or prism) and then to the detector. Grating selects different wavelengths sequentially. Thus at the detector, signal from the reference and sample arrives alternately for different wavelengths scanned by the grating. IR detector output from sample and the reference are compared and plotted as absorbed intensity versus wavelength or usually cm^{-1}.

7.6.5 Fourier Transform Infra Red Spectrometer

Fourier Transform Infra Red (FTIR) spectrometer makes use of the Michelson interferometer for recording the spectra. As shown in Fig. 7.36 a parallel beam of infra red rays falls on the beam splitter BS.

IR source and detector are similar to those used in dispersive type IR spectrometer discussed earlier. Part of the beam falls on a movable (0–1 cm) mirror M_1 and a fixed mirror M_2.

The rays are reflected back from both the mirrors along the same path and interfere at BS. A part of this combined beam falls on the sample and the detector. Constructive and destructive interference occurring at BS depends upon the path length of the rays. A white beam i.e. the beam containing a broad continuous spectrum of wavelengths produces constructive and destructive interference pattern

of every wavelength with all others. Intensity as a function of the position of movable mirror position is given by

$$I(x) = \int_{-\infty}^{\infty} I(v) \cos(2\pi x \mathrm{v})\, d\mathrm{v} \tag{7.36}$$

Inverse transform gives

$$I(v) = \int_{-\infty}^{\infty} I(x) \cos(2\pi x \mathrm{v})\, d\mathrm{v} \tag{7.37}$$

The recombined beam passing through the sample produces absorption spectrum in which certain characteristic frequencies are absorbed by molecules present in the sample.

With modern computers, it is quite an easy job to carry out a Fourier Transform. Detector collects, for example, signal from sample every millisecond and stores each spectrum in different locations. Spectra are then Fourier transformed and resultant spectra are obtained as an output. Thus, spectra can be generated very fast and Fourier Transform also is very fast. Thus better and fast data acquisition is possible using an FTIR spectrometer. Hence most of the modern commercial infrared spectrometers are FTIR spectrometers. An FTIR spectrum of TiO_2 is shown in Fig. 7.37.

7.6.5.1 Sample Preparation

Sample preparation is a difficult task in IR range as there is no transparent material for cuvettes. Alkali halides (such as NaCl, KBr) are usually used which are transparent even at longer wavelengths. Powder samples are mixed with alkali halides

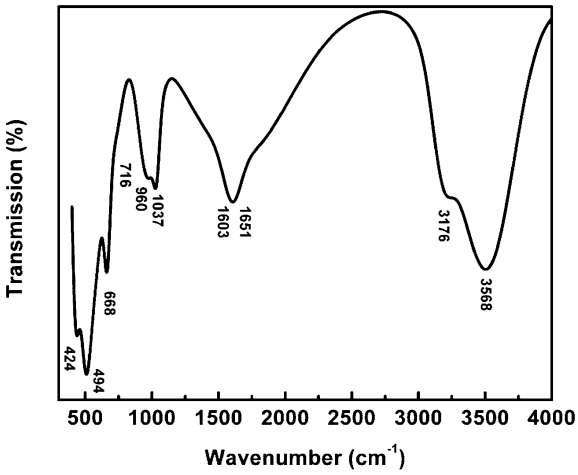

Fig. 7.37 FTIR of TiO_2, suggesting vibrations due to TiO_6 octahedron and adsorbed hydroxyl group (3,568 cm^{-1})

and pressed in the sample holder. For liquid samples, there are single crystals of KBr or NaCl and liquid is sandwiched between the two. But in this case one cannot use aqueous solutions because alkali halides are soluble in water. For such samples silver chloride is used. One can use Teflon also but it shows absorption bands for C-C and C-F. For frequencies less than 600 cm^{-1} one can use polyethylene cell also.

7.6.6 Raman Spectroscopy

Raman spectroscopy is another powerful technique for the analysis of molecules or particles. This also is sensitive to the vibration spectrum of molecules. However it is complementary to the IR analysis. Unlike IR active molecules, Raman active molecules do not depend upon the presence of a dipole moment but on the polarizability of the molecule. The technique is based on the Raman effect discovered by Sir C.V. Raman in 1928. Whenever scattering of the light occurs, the scattered light consists of two types viz. *Rayleigh scattering* and *Raman Scattering.* Rayleigh scattering is strong and has the same frequency (elastic scattering) as the incident beam (υ_0), and the other is called *Raman scattering*. Raman scattering is inelastic scattering and has frequencies $\upsilon_0 \pm \upsilon_m$ where υ_m is a vibrational frequency of a molecule. Raman scattering is very weak ($\sim 10^{-5}$ of the incident beam). The decreased frequency ($\upsilon_0 - \upsilon_m$) and increased frequency ($\upsilon_0 + \upsilon_m$) lines are called the *Stokes* and *anti-Stokes* lines, respectively. The scattering is described as an excitation of the molecule to a virtual state which is lower in energy than a real electronic transition, with nearly coincident de-excitation and a change in vibrational energy. The scattering event occurs in 10^{-14} s or less. In Raman spectroscopy, the vibrational frequency υ_m is measured as a shift from the incident beam frequency υ_0 (Boxes 7.9 and 7.10).

Box 7.9: Fourier Transform Spectroscopies

Technique of Fourier Transform is used in many spectroscopies like Raman Spectroscopy, Infra Red Spectroscopy, and Nuclear Magnetic Resonance Spectroscopy. It collects simultaneously the data at various frequencies and is much superior to conventional way of sequentially scanning different frequencies (or wavelengths). Fourier Transform is a mathematical method and is capable of resolving complex spectrum into various frequencies as follows.

Consider that two sine waves of different wavelengths have mixed as shown in Fig. 7.38a. They have different frequencies and their sum would appear as in Fig. 7.38b. A Fourier Transform of the resultant waves gives two separate frequencies as showed in Fig. 7.38c.

(continued)

Box 7.9 (continued)

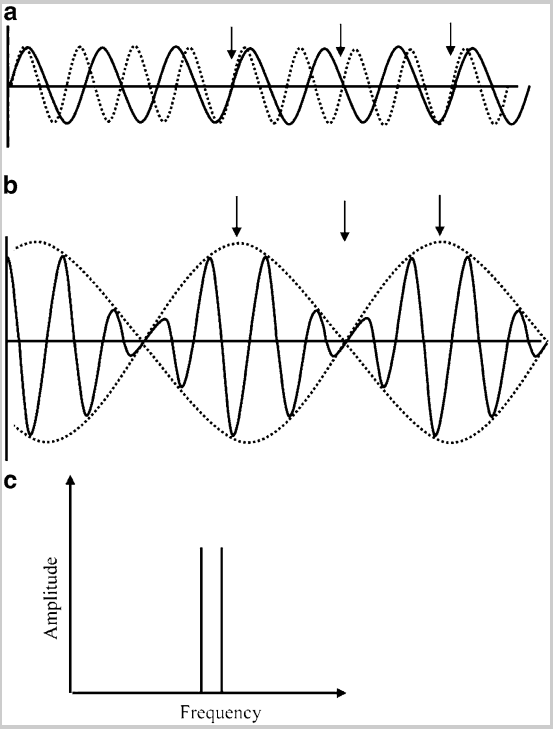

Fig. 7.38 Fourier transform of two waves having different frequencies. Fourier Transform bears its name due to Jean Baptiste Fourier, a French mathematician who developed this procedure in early 1800

Box 7.10: C.V. Raman

C.V. Raman was born on 7th November 1888 in a city Tiruchirapalli in Tamil Nadu, India. His full name is Chandrasekhara Venkata Raman. His father was a Professor in Mathematics and Physics. Born in a highly educated family Raman was known as a very bright student. He joined Presidency College in Madras (now known as Chennai) in 1902 and received B.A. degree in 1904 bagging Gold Medal in Physics. In 1907 he received M.A. degree with distinction. Immediately he joined Indian Finance Department in 1907 as the conditions prevailing in India were such that even a bright student like Raman had no proper opening in science. In spite of this, young Raman did not lose his passion for science and continued his experiments after his office hours. He used to regularly visit Indian Institute of Cultivation of Science and pursue the experiments in light scattering. Later in 1917, he was

(continued)

Box 7.10 (continued)
offered a prestigious position of Sir Tarakanath Palit Professorship in Calcutta University. He remained with Calcutta University for 15 years during which period he became known all over the world as a great scientist.

His recognition started with prestigious Fellowship of Royal Society of London in 1924. He was made 'Knight of British Empire' in 1929. In 1930 he received the Nobel Prize for his discovery of the light scattering effect known as 'Raman Effect' after him. He is the only Indian scientist to receive this honour. He became the director of Indian Institute of Science, Bangalore in 1934. In 1949 he established in Bangalore 'Raman Research Institute', one of the well known institutes of India. Raman received 'Bharat Ratna' award from Government of India and Lenin Peace Prize in 1957 to name a few amongst the various honours. Raman was not only interested in the light scattering but also in acoustics particularly science of musical instruments. Raman was a great lover of diamonds and other stones and had a huge collection of them which he turned into a museum in Raman Research Institute. Raman died on 21st November 1970.

A Raman spectrometer comprises four components which are: (1) excitation source (laser), (2) sample illumination and collection system, (3) wavelength selector and (4) detector and computer processing system. FT-Raman spectrometer is preferred over the normal Raman spectrometer due to the advantage of measuring information of all frequencies at the same time. The instrumentation of FT-Raman is similar to normal Raman spectrometer with an additional inclusion of a Michelson interferometer, which enables the simultaneous acquisition of signals of all frequencies along with the improved resolution. Figure 7.39 shows a schematic of a typical FT-Raman spectrometer. The laser is incident on the sample by means of a lens and a parabolic mirror. The scattered light from the sample is collected and passed to a beam splitter and to the moving and fixed mirrors in the interferometer head. It is then passed through a series of filters and focused onto a liquid-nitrogen-cooled detector.

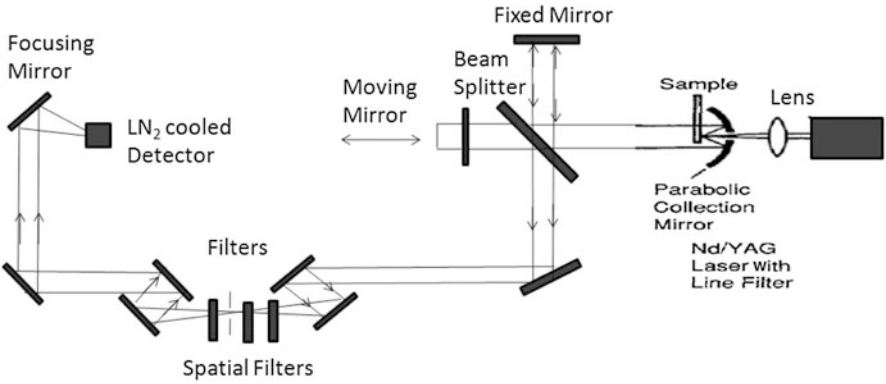

Fig. 7.39 Schematic diagram of FT-Raman spectrometer

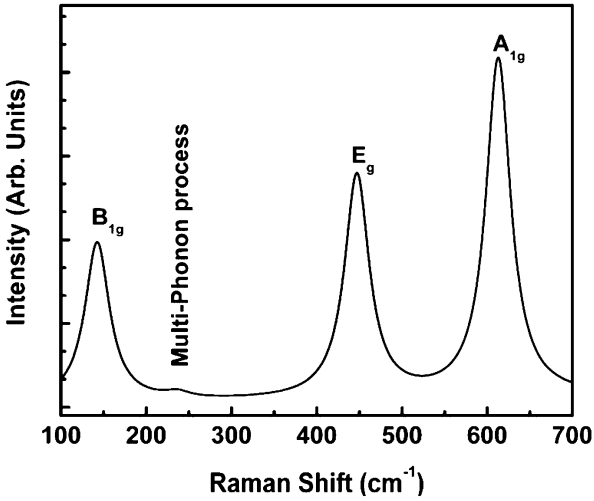

Fig. 7.40 Raman spectrum of TiO_2. Different modes of vibrations can be seen which are characteristic of rutile phase of TiO_2

Raman spectra are shown as 'Raman shift'. Raman spectra are considered to be indispensable for carbon nanotubes and other carboneous materials as amorphous, crystalline etc. characteristic forms can be easily identified. Figure 7.40 depicts the Raman spectrum for rutile TiO_2.

7.6.7 Luminescence

Some materials when excited with an external source of stimulus like electrons or light emit light in the visible range, UV or IR. This phenomenon is known as *luminescence.* The word luminescence was coined by E. Wiedermann in 1888 from a Latin word *lumen* which means *light*. The word luminescence includes

fluorescence and *phosphorescence.* They differ in the duration of time over which light is emitted. Usually, the terminology fluorescence is used if the emission of light takes place within $\sim 10^{-4}$ s of stimulus. If the emission persists for a longer duration of few tens of milliseconds to $\sim$10 s after the stimulus is removed it is termed as phosphorescence. Phosphorescence is sometimes also called as *afterglow*.

Many nanomaterials exhibit enhanced (increased intensity) luminescence as compared to their bulk counterparts. Some materials like silicon which are not luminescent in their bulk form become luminescent in nano form, like porous silicon (discussed in Chap. 11). Therefore luminescence investigations of nanomaterials are often carried out.

There are various types of luminescence like photoluminescence, cathodoluminescence, electroluminescence and so on depending upon the external stimulus used to excite the material. Luminescence investigations are useful to analyse the electronic structure of the material. It not only gives information about the transitions between conduction and valence band but also the localized states due to impurities or doping. We shall discuss their details in Chap. 8. Here we shall consider only the experimental technique to obtain photoluminescence. Further it should be mentioned that we discuss here only necessary parts of the spectrometer and actual instrument may be quite elaborate.

7.6.7.1 Photoluminescence Spectrometer

A schematic diagram of photoluminescence set up is shown in Fig. 7.41 which can be suitably modified to observe other types of luminescence by using the relevant source of excitation in place of photon source. Basically there has to be

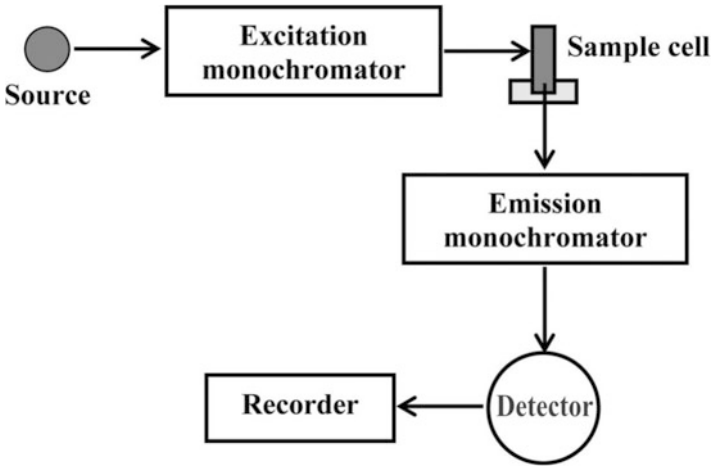

Fig. 7.41 Schematic layout of photoluminescence set up

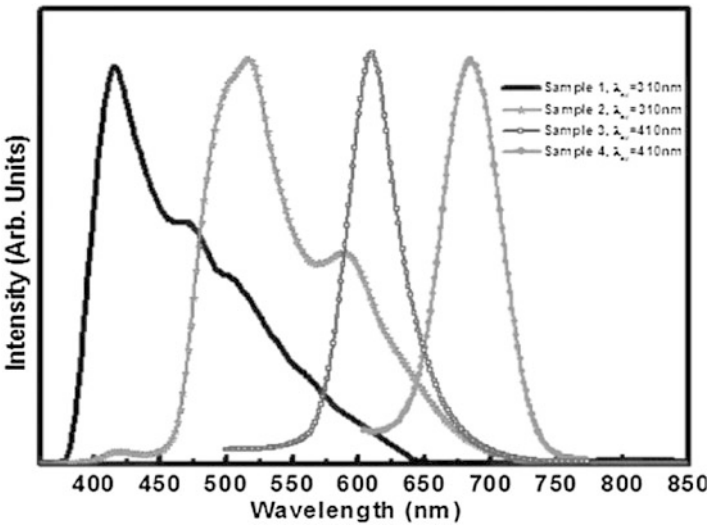

Fig. 7.42 Photoluminescence spectra from CdSe nanoparticles of two different sizes

a source of photons ranging from UV (∼200 nm) to IR (∼800 nm), a filter to throw away large band of wavelengths, wavelength selectors or monochromators, sample holder, a detector and a recording system like an X-Y recorder or a computer. Two types of arrangements viz. transmission type and reflection type layouts are normally used. The transmission type of geometry is, however, unsuitable for solid samples.

Figure 7.42 illustrates an example of a photoluminescence spectrum obtained from CdSe nanoparticles of different qualities and sizes.

7.6.8 X-Ray and Ultra Violet Photoelectron Spectroscopies (XPS or ESCA and UPS)

X-ray Photoelectron Spectroscopy (XPS), popularly known as Electron Spectroscopy for Chemical Analysis (ESCA), was developed by K. Siegbahn. A large number of books and reviews are available on ESCA. The technique is based on the photoelectric effect, as explained by Einstein in 1905. Accordingly (Fig. 7.43), photon of fixed energy $h\nu$ incident on an atom ejects an electron of binding energy E_B with kinetic energy E_K according to the equation

$$h\nu = E_K + E_B \tag{7.38}$$

Knowing $h\nu$ and by measuring with an energy analyzer, the kinetic energy E_K of electron, binding energy of electron in an atom can be determined. The equation is

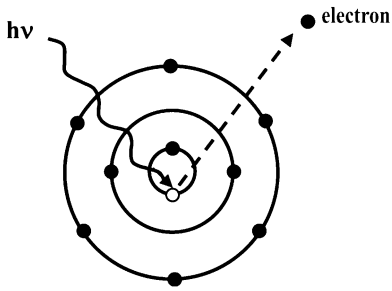

Fig. 7.43 Schematic of photoemission

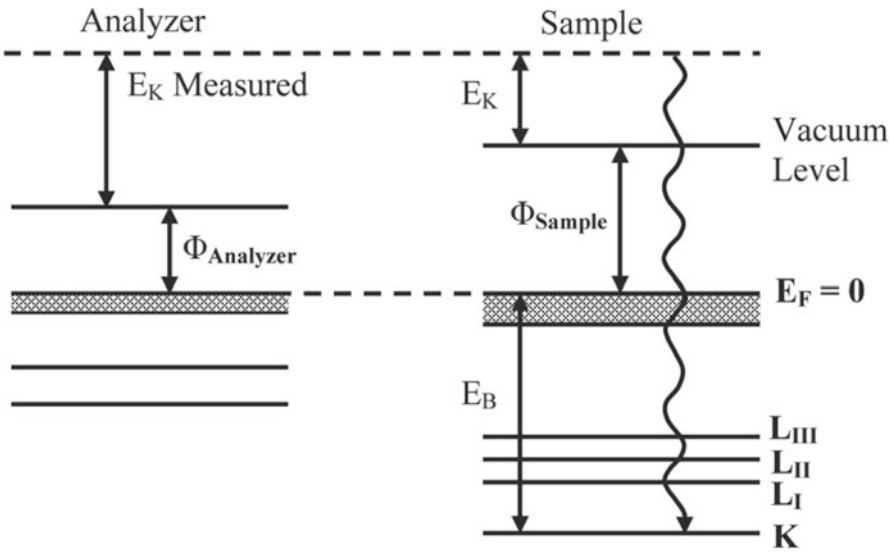

Fig. 7.44 Energy level diagram for photoelectron spectroscopy of solids

valid for atoms in gases, liquids or solids. In a solid (see Fig. 7.44), additional energy (ϕ) the work function of the solid is required for the electron to get emitted as

$$h\nu = E_K + E_B + \phi \tag{7.39}$$

Work function of solids changes from material to material. It also depends on their cleanliness and purity. Fortunately, it is not necessary to know ϕ of the solid. Kinetic energies of emitted electrons are measured with reference to Fermi level and ϕ can be replaced by ϕ_{SP}, the work function of the spectrometer. Therefore, one gets the measured E_K, which differs from the kinetic energy of photoelectron coming out from the sample. When Fermi level of the sample and the analyzer are aligned (by keeping both at earth potential) there is a constant difference between measured kinetic energy and the kinetic energies of electrons emitted from different

samples. As the work function of the spectrometer is known, it is not necessary to know the work function of the samples and one can easily find out the kinetic or binding energies of the samples.

One obtains intensity of electrons versus electron energy which is the Electron Distribution Curve (EDC). Core level electrons in atoms of the solid are very sensitive to their neighbouring atoms. Therefore analysis of photoelectrons was originally known as 'Electron Spectroscopy for Chemical Analysis'. However, there are many electron spectroscopies available now, which yield chemical information. It is therefore safer to call the technique as X-ray Photoelectron Spectroscopy (XPS), which specifically indicates that photoelectrons are produced using X-rays.

When an electron is ejected from a solid sample, a hole is created. Binding energy measured, therefore, gives the energy of the photoelectron in presence of the hole. When an electron leaves an atom, remaining electrons of the atom (and even the surrounding atoms) interact with the hole. The interaction energy depends on the atomic number as well as the energy level in which the hole resides. Corresponding relaxation energies can be large. Thus binding energies measured in an experiment are not the initial state energies of photoelectrons as depicted in Eq. (7.39). However, measured binding energies are still quite useful as they are characteristic binding energies of a given element. As mentioned earlier, the photoelectrons have energies which are quite sensitive to their local environment. Thus measurement of binding energies results into useful chemical information.

7.6.8.1 Ingredients of X-Ray Photoelectron Spectra

Photoelectron spectra are usually rich in their contents. Following ingredients can be made use of in understanding the properties of materials.

(i) Chemical shift
(ii) Valence band
(iii) Auger peaks
(iv) Spin-orbit splitting
(v) Multiplet splitting
(vi) Satellites
(vii) Plasmon loss

Origin of these features is briefly described below. Details can be found in some review articles on XPS.

Chemical shift – Core electrons of atoms in solids are very sensitive to their surrounding. Whenever there is a charge transfer between outer electrons of different atoms, core electrons also respond to these changes by changing their energies. Thus, there are changes in the binding energies of electrons in a solid. These changes can be studied by analyzing the kinetic energies of photoelectrons.

Valence band – Photoelectron spectroscopy using X-rays or UV rays from helium can be used to infer about the density of states in the vicinity of Fermi level. Photoemission cross-sections are very sensitive to photon energy. Taking advantage

of the situation that in typical commercial instrument Al K_α (1,486.6 eV), Mg K_α (1,253.6 eV), He I (21.2 eV) and He II (40.8 eV) sources of widely different energies are present, useful cross-section dependent analysis can be made. Valence band spectra show considerable changes when recorded with different photon energies.

Auger peaks – Along with photoelectron peaks, some Auger peaks characteristics of elements present in the solid also can be obtained in a spectrum. Origin of Auger peaks will be discussed in the next sub-section.

Spin-orbit splitting – Some of the peaks in photoelectron spectra appear as doublets. These are due to splitting of p shells [$2p_{3/2} - 2p_{1/2}$, $3p_{3/2} - 3p_{1/2}$ etc.] as well as d and f sub-shells. Spin-orbit splitting for a given atom decreases with increase in the principal quantum number. It increases for a given principal quantum number with increase in atomic number. For large atomic number compounds, spin-orbit splitting can be used for finding out the oxidation state. Spin-orbit splitting differences are quite large for oxides of high Z atoms compared to pure forms.

Multiplet splitting – Large magnetic moments on some of the atoms/ions arise due to unpaired electrons in their 3*d*, 4*d* or 4*f* shells. Photoelectron spectroscopy can be used to detect the presence of such unpaired electrons. For example, in Fe^{3+} there are two paired electrons in 3 *s* level and five unpaired electrons with parallel spins in 3*d* level. When photoelectron is ejected from 3 *s* level two situations can arise viz. (a) an electron left in 3 *s* is parallel to electrons in 3*d* level or (b) antiparallel to 3*d* electrons. The energy difference due to situation in (a) and (b) can be as large as few electron volts and depends upon the number of electrons in *d* level. In fact, both the cases have certain probability to exist. Therefore 3 *s* photoelectron spectrum exhibits two peaks. Splitting of 3 *s* levels can be correlated to electrons in *d* level and becomes a measure of magnetic moment.

Plasmons loss – Photoelectrons with large kinetic energy can excite plasmons (plasmons are collective but quantized oscillations of electrons in a solid) with energy

$$\omega_p^2 = \frac{4\pi N e^2}{m} \text{ (C.G.S.)} \tag{7.40}$$

where ω_p is plasmon frequency, n – number of electrons per cm^3 and m* is the effective mass of electron. In such a case, photoelectron peaks are accompanied by peaks on their higher binding energy side. Bulk plasmon peaks along with second and higher harmonics can be observed with decreasing intensity. Surface plasmon peaks at energies $\omega_p/\sqrt{2}$ also can be observed.

Satellites – Intense or weak peaks can some times be observed along with main photoelectron peak. Origin of these peaks can be understood in terms of electron shake up, shake off or charge transfer and many body interactions collectively referred to as satellites. In the process of photoelectron emission, a hole is created. Remaining electrons respond to this by monopole excitation to a discrete level (shake up) or continuum (shake off). The energy for excitation is derived from outcoming photoelectron. Such photoelectron appears as a peak on the higher binding energy with respect to the ones that come without losing energy.

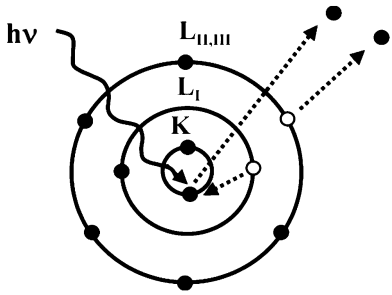

Fig. 7.45 Schematic of an Auger process

7.6.9 Auger Electron Spectroscopy

Auger electrons were discovered by P. Auger in 1925 but their potential for surface analysis was realized after few decades. As illustrated in Fig. 7.45, when one of the electrons from a core level is removed, an electron from outer level combines with the core hole. The energy difference between the two levels is either emitted as X-ray (photons) or utilized in emitting an electron from one of the outer levels. An electron removed by the later process is known as Auger electron. It is a three-level process and as can be seen from the illustration, three electrons are necessary for the Auger process to take place. Therefore, except H, He and Li, all the elements can produce Auger electrons. Energy of an Auger electron in Fig. 7.45 can be written as

$$E_{K,LI,LII\text{-}III} = E_K - E_{LI} - E_{LII\text{-}III} \tag{7.41}$$

where E_K, E_{LI} and $E_{LII\text{-}III}$ are binding energies of electrons in K, L_I and $L_{II\text{-}III}$ levels respectively. Emissions of photons and Auger electrons are competing processes.

Production of core hole for emitting Auger electron is independent of the process in which core hole is created. Photons, electrons or even ions can be used to produce core hole. Auger electrons are therefore produced along with photoelectrons. Auger electrons are characteristics of atom from which they are released and are useful in the elemental analysis. One can use electrons, photons or even ions to produce Auger electrons. More details can be found elsewhere in some review article on Auger spectroscopy.

7.6.9.1 Surface Sensitivity of Photoelectron and Auger Electron Spectra

Photoelectron spectroscopy can be performed using X-rays or Ultra Violet (UV) rays. X-rays and UV rays can penetrate from few micrometres or fraction of a micrometre depth depending upon the energy of the radiation. However, electrons have much shorter mean free path in solids. Therefore, even if photoelectrons can be generated deep within a solid, few electrons can escape out of solid, depending upon their kinetic energy. An empirical curve of electron escape depth as a function

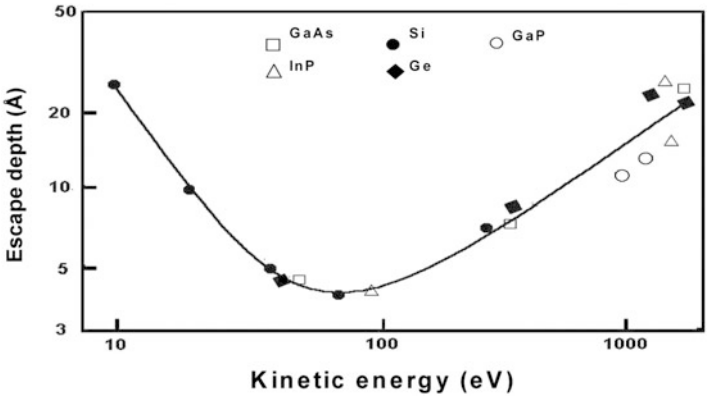

Fig. 7.46 Dependence of escape depth of electrons on kinetic energy

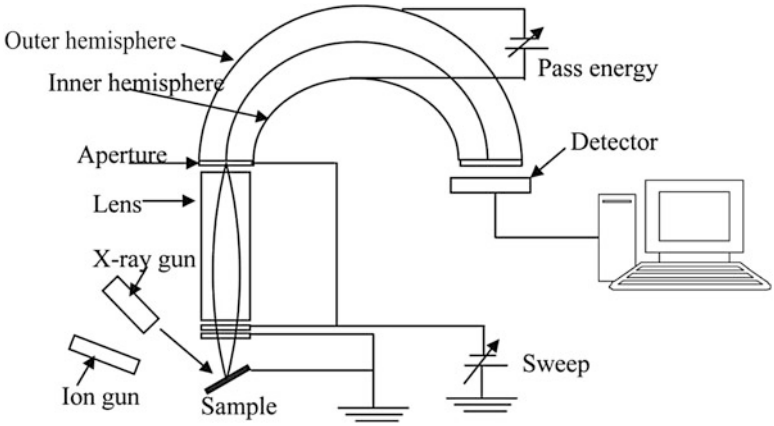

Fig. 7.47 Schematic of ESCA using CHA

of their kinetic energy is shown in Fig. 7.46. It can be seen that if the electron kinetic energy is around 100–200 eV, escape depth of the electrons is very small, less than a nanometer.

One can always find for a given photon source, some photoelectrons from core or shallow energy level which will come from few nano or sub nanometer depth. Thus photoelectron spectroscopy is a surface sensitive technique. Same is true for Auger electrons.

7.6.9.2 Experimental Set Up

In Fig. 7.47, basic requirements of photoelectron and Auger spectroscopy are illustrated. Except for the source of excitation, instrumentation required by both the techniques is same. This is very useful. AlK_{α} with photon energy 1,486.6 eV and

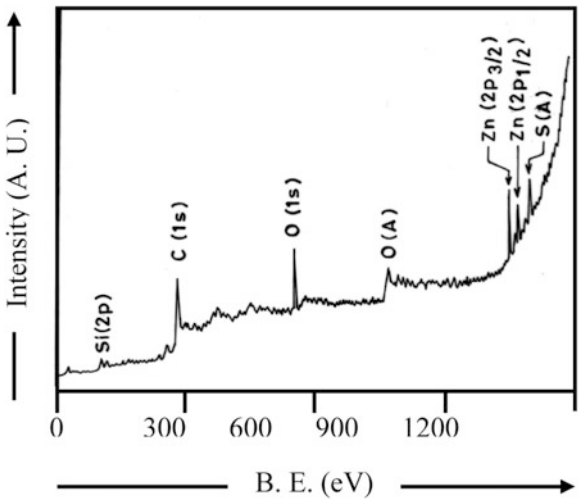

Fig. 7.48 XPS spectrum of ZnS sample obtained using MgK_α source

MgK_α with photon energy 1,253.6 eV are available from a twin anode as source of X-rays. Alternatively, a helium discharge lamp also can be used to emit HeI and HeII with photon energies 21.2 and 40.8 eV respectively. HeI and HeII are obtained by operating the UV discharge lamp with helium gas flowing in it.

Auger electrons can be a part of photoelectron spectrum. However, it is common to use an electron gun (2–5 keV) as the source of incident electrons to create core holes. Electrons have the advantage that they can be generated easily and focused to a small spot. They also can be rastered on the sample surface.

Photoelectrons and Auger electrons are analyzed in the same analyzer using Concentric Hemispherical Analyzer (CHA) or double pass Cylindrical Mirror Analyzer (CMA). Analyzer is controlled using spectrometer control unit (SCU). Electrons passing through them are selected according to their energies, are detected and amplified using channeltron or channel plate. Amplified signal after suitable noise filtering is an input for an X-Y recorder or a computer. An X-Y plot or a spectrum of intensity versus electron kinetic/binding energy can be obtained. One can make use of readily available data books to identify the elements (Fig. 7.48).

Core levels due to elements present in the sample are marked on Fig. 7.49. Besides the prominent peaks, a number of other peaks appear on high binding energy sides. They also are useful in understanding electronic structure of the sample. A typical Auger spectrum can be seen in Fig. 7.49.

7.7 Magnetic Measurements

7.7.1 Vibrating Sample Magnetometer (VSM)

Using this technique, magnetization of a sample on application of magnetic field can be measured. Other sensitive technique is Superconducting Quantum Interference

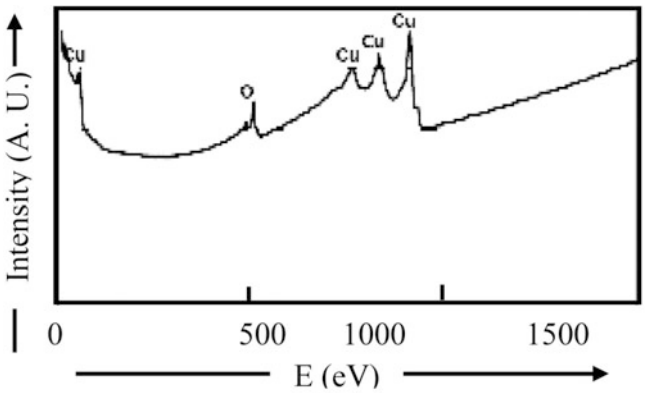

Fig. 7.49 Auger spectrum of Cu sample

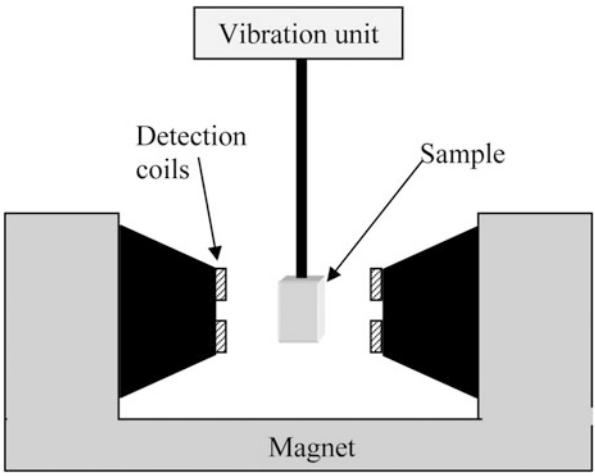

Fig. 7.50 Schematic diagram of VSM

Device (SQUID), not discussed here. The instrument is based on the principle that an oscillatory magnetic field can be created by vibrating a magnetic sample. Magnetization in the sample is induced by applying a uniform magnetic field to the sample. The induced changes in the magnetic field are detected by a search coil. Applied magnetic field is usually quite large, but being constant is not detected by search coil. Generally the constant magnetic field is not really constant but slowly varied so that induced magnetization in the sample at different fields can be investigated. One can assume this slowly varying magnetic field as constant compared to vibrating field (Hz). Figure 7.50 gives the schematic diagram of a typical VSM. In most of the standard set ups a large electromagnet with 0 to 2.5 T field is used, although much higher magnetic field also can be provided. The pole pieces of the electromagnet are such that a large uniform magnetic field prevails for a sample, may be a thin film or powder sample held in a glass capillary attached to a special drive.

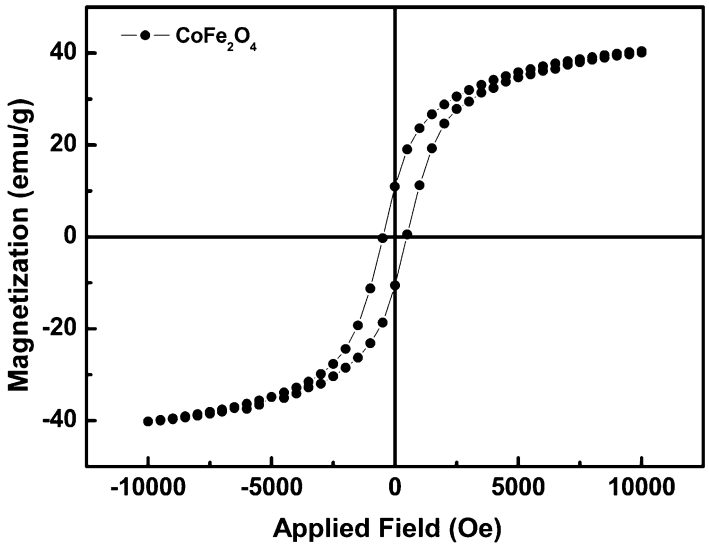

Fig. 7.51 M-H plot for $CoFe_2O_4$ nanoparticles

Paramagnetic, diamagnetic, ferromagnetic and other samples can be distinguished by plotting magnetization versus applied magnetic field. Provision can be made to heat or cool the samples during magnetic measurements. This enables one to study magnetic phase transitions.

In Fig. 7.51, the hysteresis curve obtained for $CoFe_2O_4$ nanoparticles obtained using a VSM is shown.

7.8 Mechanical Measurements

Mechanical properties like elastic properties, hardness, ductility or friction of different nanostructures need to be investigated. It should be, however, noted that measurements on single nanoparticles, rods or tubes would inherently be difficult, though not impossible. However measurements on nanocrystalline solids, thin films etc. are possible using some conventional methods. Techniques like nanoindentation are available. Before discussing about it let us first revise some of the concepts in mechanical properties.

7.8.1 Some Common Terminologies Related to Mechanical Properties

Mechanical properties of materials can be understood from Young's modulus, toughness and hardness.

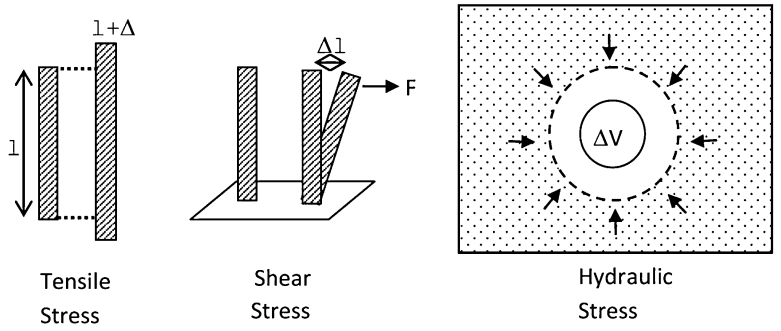

Fig. 7.52 Different types of stresses

$$\textbf{Young's modulus}: Y = \text{stress}/\text{strain} \tag{7.42}$$

It is a measure of elongation (deformation) in the limit of small stress.

Plastic deformation: When the material is elongated further, it may break. Before breaking, it can exhibit non-linear behaviour which can be described as plastic deformation.

Toughness: It is the amount of work necessary for mechanical failure of the material. It is thus a measure of energy that can be absorbed by the material. Both linear and non-linear contributions need to be taken into account to determine the toughness. Area under stress-strain curve is a measure of toughness.

Stiffness: Greater the modulus of elasticity, stiffer is the substance.

Ductility: It is the plastic deformation that can be sustained at fracture.

Hardness: Material's resistance to deformation or to produce indentation or abrasion.

Elastic Moduli: In some solids atoms are arranged such that the objects are stiff or rigid. For example, glass, table and ceramic cup are rigid. On the other hand, some objects are flexible like thread, plastic bag, garden hose in which atoms are arranged in long flexible chains. However all objects are elastic to some extent i.e. their dimensions can be changed (strain) by application of force (stress). There are various types of stresses viz. tensile stress, shear stress and hydraulic stress depending upon the direction of stress and strain as illustrated in Fig. 7.52.

Young's Modulus (Y):

$$Y = \frac{Stress}{Strain} \tag{7.43}$$

Tensile and compression strength can be different. For example cement has large compressive strength but poor tensile strength (Fig. 7.53).

Shear Modulus (G):

$$G = \frac{\text{Stress}}{\text{Strain}} \tag{7.44}$$

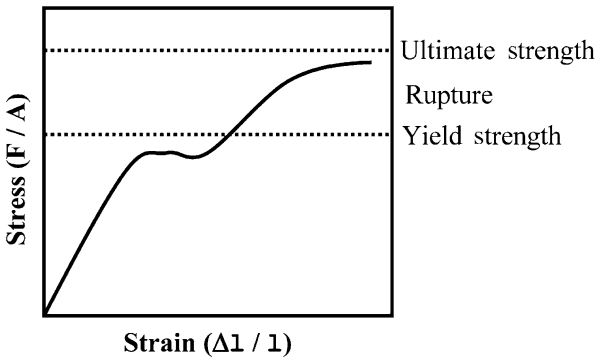

Fig. 7.53 Relation between stress and strain

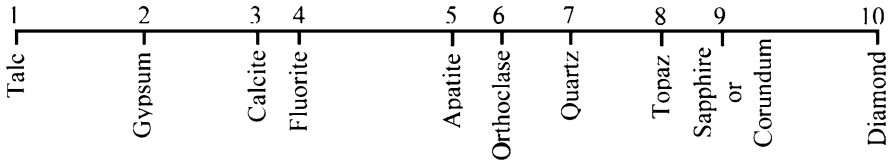

Fig. 7.54 Hardness of some standard minerals

Bulk Modulus (B):

$$B = \frac{P}{\Delta V / V} \tag{7.45}$$

Hardness: Hardness is one of the important mechanical properties of solid materials. It is a measure of a material's ability to resist local, plastic deformation.

There are different scales to measure hardness viz. Brinell hardness test, Rockwell hardness test, Knoop's hardness test, Vicker's hardness test and Mohs hardness test. Out of these, Mohs hardness test is one of the oldest and gives a scale from 1 to 10. One is for the softest material viz. talc and ten is for the hardest materials viz. diamond. The middle numbers, 2–9 are related to different minerals as standards of hardness as shown in Fig. 7.54.

The scale is based on the ability of harder material to scratch the softer material.

Other hardness tests are quantitative. They are based on the specific indentors used to scratch the material to be tested for the hardness. A controlled load determines the depth and size of the indentation in the material under test.

Vicker's Hardness (VHN) test is often used in which a small diamond indentor is used. It has a pyramid shape (See Fig. 7.55). The resulting impression of the diamond is observed under a microscope and used to determine the VHN.

Nanomechanical properties are measured using a 'nanoindenter' integrated with an atomic force microscope (AFM). In the conventional techniques, a hard tip is pressed in the material under certain known load and the load is removed after some time. The impression left behind in the material is investigated

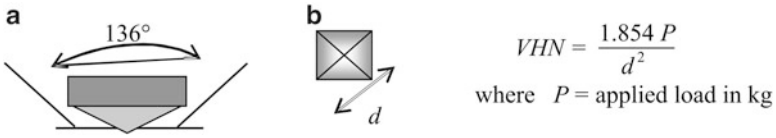

Fig. 7.55 (**a**) Pyramid shaped diamond tip and (**b**) *top view* of the typical impression of the tip in the material

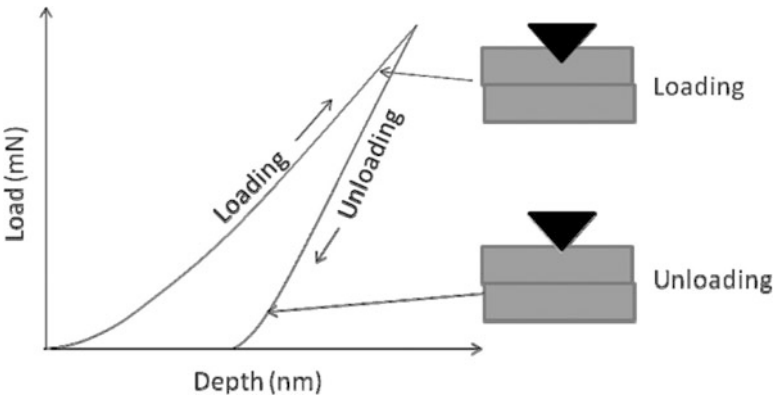

Fig. 7.56 Nanoindentation method

(area of the impression) using a suitable microscope. In nanoindentation, force and displacement of the tip in the material are continuously monitored. The depth of tip penetration as a function of load gives rise to a 'loading' curve (see Fig. 7.56). The tip movement is also monitored while 'unloading' leading to complete history of the displacement. Typical loads are upto about 500 mN and displacements upto 50 μm.

Using nanoindentors, it is possible to investigate mechanical properties like hardness, modulus of elasticity, creep and plastic flow.

Further Reading

T.A. Carlson, *Photoelectron and Auger Electron Spectroscopy* (Plenum Press, New York, 1978)
B.D. Cullity, S.R. Stock, *Elements of X-Ray Diffraction*, 3rd edn. (Prentice Hall, Upper Saddle River, 2001)
H.H. Willard, L.L. Merritt Jr., J.A. Dean, F.A. Settle, *Instrumental Methods of Analysis*, 7th edn. (CBS Publishers, New Delhi, India, 1986)
J.B. Wachtman, Z.H. Kalman, *Characterization of Materials* (Elsevier/Butterworth-Heineman, Boston, 1993)